ORNL/TM-10867

ornl

OAK RIDGE
NATIONAL
LABORATORY

MARTIN MARIETTA

Triple Ion Beam Irradiation Facility

M. B. Lewis
W. R. Allen
R. A. Buhl
N. H. Packan
S. W. Cook
L. K. Mansur

OPERATED BY
MARTIN MARIETTA ENERGY SYSTEMS, INC.
FOR THE UNITED STATES
DEPARTMENT OF ENERGY

Printed in the United States of America. Available from
National Technical Information Service
U.S. Department of Commerce
5285 Port Royal Road, Springfield, Virginia 22161
NTIS price codes—Printed Copy:A05 Microfiche A01

ORNL/TM-10867

Metals and Ceramics Division

TRIPLE ION BEAM IRRADIATION FACILITY

M. B. Lewis, W. R. Allen, R. A. Buhl, N. H. Packan,
S. W. Cook, and L. K. Mansur

Date Published: December 1988

Prepared for
DOE Office of Basic Energy Sciences
KC 02 01 05 0

Prepared by the
OAK RIDGE NATIONAL LABORATORY
Oak Ridge, Tennessee 37831-6285
operated by
MARTIN MARIETTA ENERGY SYSTEMS, INC.
for the
U.S. DEPARTMENT OF ENERGY
under contract DE-AC05-84OR21400

TABLE OF CONTENTS

LIST OF FIGURES

TRIPLE ION BEAM IRRADIATION FACILITY*

M. B. Lewis, W. R. Allen, R. A. Buhl,
N. H. Packan, S. W. Cook, and L. K. Mansur

ABSTRACT

A unique ion irradiation facility consisting of three accelerators is described. The accelerators can be operated simultaneously to deliver three ion beams on one target sample. The energy ranges of the ions are 50 to 400 keV, 200 keV to 2.5 MeV, and 1.0 to 5.0 MeV. Three different ions in the appropriate mass range can be simultaneously implanted to the same depth in a target specimen as large as 100 mm^2 in area. Typical depth ranges are 0.1 to 1.0 μm. The X-Y profiles of all three ion beams are measured by a system of miniature Faraday cups. The low-voltage accelerator can periodically ramp the ion beam energy during the implantation. Three different types of target chambers are in use at this facility. The triple-beam high-vacuum chamber can hold nine transmission electron microscopy specimens at elevated temperature during an irradiation by the three simultaneous beams. A second high-vacuum chamber on the medium-voltage accelerator beamline houses a low- and high-temperature translator and a two-axis goniometer for ion channeling measurements. The third chamber on the high-energy beamline can be gas-filled for special stressed specimen irradiations. Special applications for the surface modification of materials with this facility are described. Appendixes containing operating procedures are also included.

1. INTRODUCTION

Ion irradiation is a modern technique used for the near-surface modification and characterization of materials. There are at least three major efforts in the ion irradiation field: (1) ion implantation and mixing used to alter the chemical environment in the matrix of atoms in a given substrate; (2) ion irradiation damage used to alter the

*Research sponsored by the Division of Materials Sciences, U.S. Department of Energy under contract DE-AC05-84OR21400 with Martin Marietta Energy Systems, Inc.

defect concentration and microstructure in the matrix or lattice of the target substrate; and (3) ion beam analysis used to characterize the stoichiometry, defects, and lattice positions of atomic mixtures in a sample substrate.

Ion implantation and mixing was first exploited by the semiconductor industry to carry out doping of silicon by a well-controlled and well-characterized low-temperature process. The success of ion implantation in the semiconductor industry has led to studies of implantation into many materials other than semiconductors. Such experiments have shown that the properties of surfaces with regard to such phenomena as friction, wear, fatigue, and corrosion can be changed by ion implantation, and exciting possibilities for improving the functional capability of materials in a variety of applications have been uncovered.[1]

Ion irradiation can produce atomic displacement damage in materials at very high rates without generating radioactivity. This has led to the use of ion beam irradiation to supplement reactor neutron irradiation for studying mechanisms leading to such phenomena as swelling, irradiation creep, solute segregation phase instability, and embrittlement of structural materials of future fusion and advanced fission reactors. In order to simulate the effects of helium gas, which is also generated along with displacements by reactor neutrons in transmutation reactions, the technique of dual ion irradiation was developed; in this case, a heavy ion beam generates displacement damage while helium from a second ion beam is simultaneously implanted in the damaged region of the target. The details of this technique have been previously described.[2]

Numerous analytical techniques use directed ion beams to measure the chemical or defect concentration versus depth profiles near the surface of test samples. Typical techniques include Rutherford backscattering (RBS), nuclear reaction analysis (NRA), proton-induced X-ray emission (PIXE), and ion channeling.[3] These techniques are often most advantageous when used in conjunction with ion implantation. The atomic mixing and defect generation that accompany ion implantation can also be quantitatively characterized by these analytical methods.

The facility described in this work was designed with the purpose of carrying out original research in all of the previously mentioned ion irradiation areas. This triple ion beam facility is an upgrade of our previously reported[2] *dual* ion beam facility. In addition to the installation of a third ion accelerator, we describe new target chamber developments and the incorporation of the Auger electron spectroscopy technique for measuring surface modifications caused by energetic ion beams. Future target chamber design and the unique applications of the new triple-beam facility are also addressed.

2. ACCELERATORS

2.1. ARRANGEMENT OF ACCELERATORS

An overall view of the Triple Ion Irradiation Laboratory is shown in Fig. 1. A simplified top view of the beamline geometry is shown in Fig. 2. The accelerators are located on two floors of the laboratory. A vertical 5-MV Van de Graaff [(a) in Fig. 1] is located on the second floor, and both horizontal Van de Graaffs, 2.5 MV [(q) in Fig. 1] and 0.4 MV [(o) in Fig. 1], are located directly below the 5-MV machine on the first floor.

All three beamlines are located on the first floor and converge at the damage target chamber [(a) in Fig. 1]. The vertical ion beam from the 5-MV accelerator is bent 90° to horizontal by the analyzing magnet [(d) in Fig. 1]. In Fig. 2, the beamline from the 400-kV machine is essentially normal to the actual target, whereas the beamlines from the remaining accelerators are at about 15° on each side of the 400-kV line. The ion beam from the 2.5-MV accelerator is analyzed by a 30° bending magnet, whereas that from the 400-kV accelerator is analyzed by a 15° magnet.

2.2. THE 5.0-MV ACCELERATOR AND BEAMLINE

The type "CN" (1.0- to 5.0-MV) Van de Graaff was originally built by High Voltage Engineering Corporation (HVEC) in the early 1950s. In the early years it was used for nuclear physics studies. Since then it has undergone several modifications, especially with regard to its ion source.

ORNL DWG 87-8756

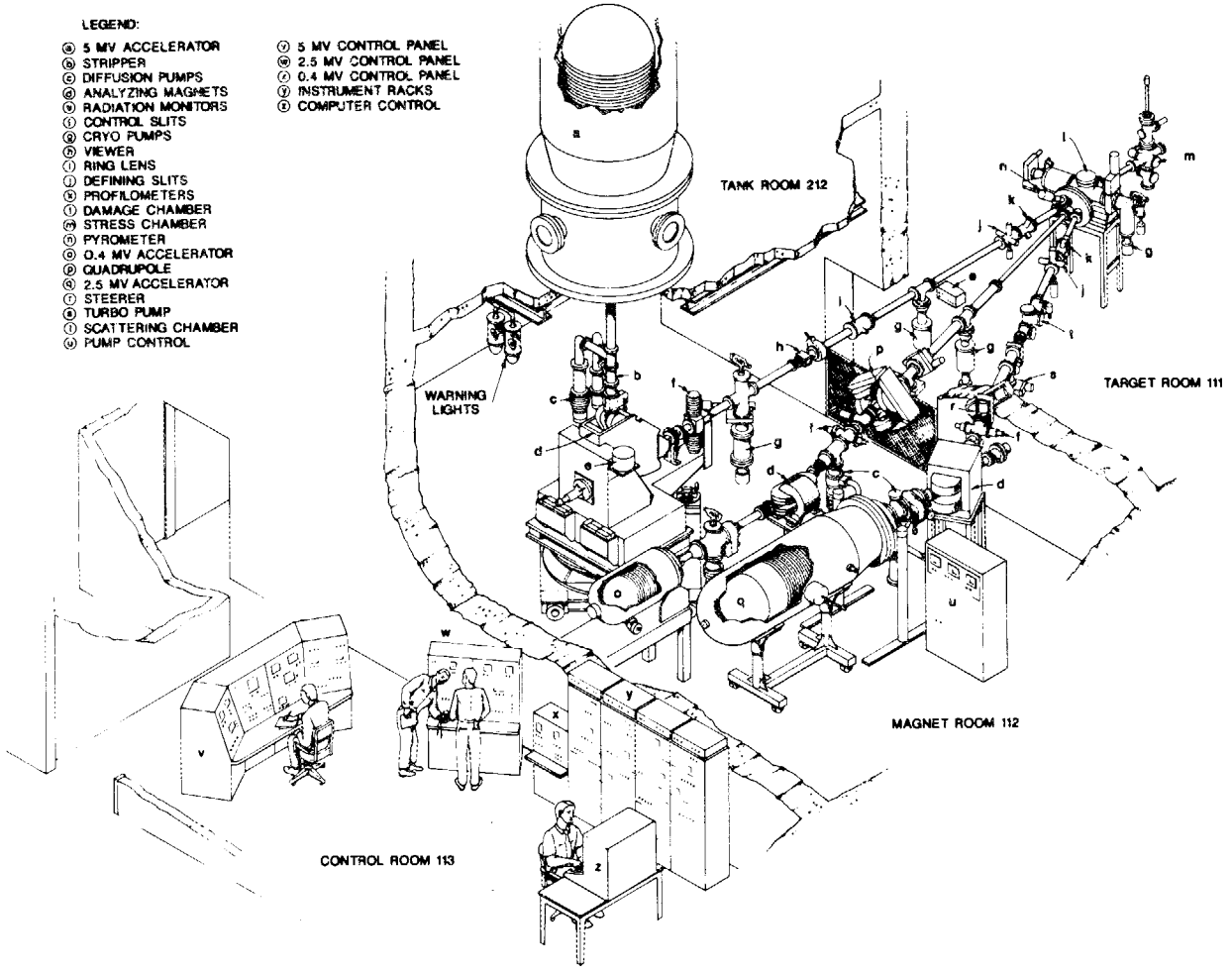

Fig. 1. A three-dimensional illustration of the Triple Ion Irradiation Laboratory. The three accelerators are labeled a, q, and o.

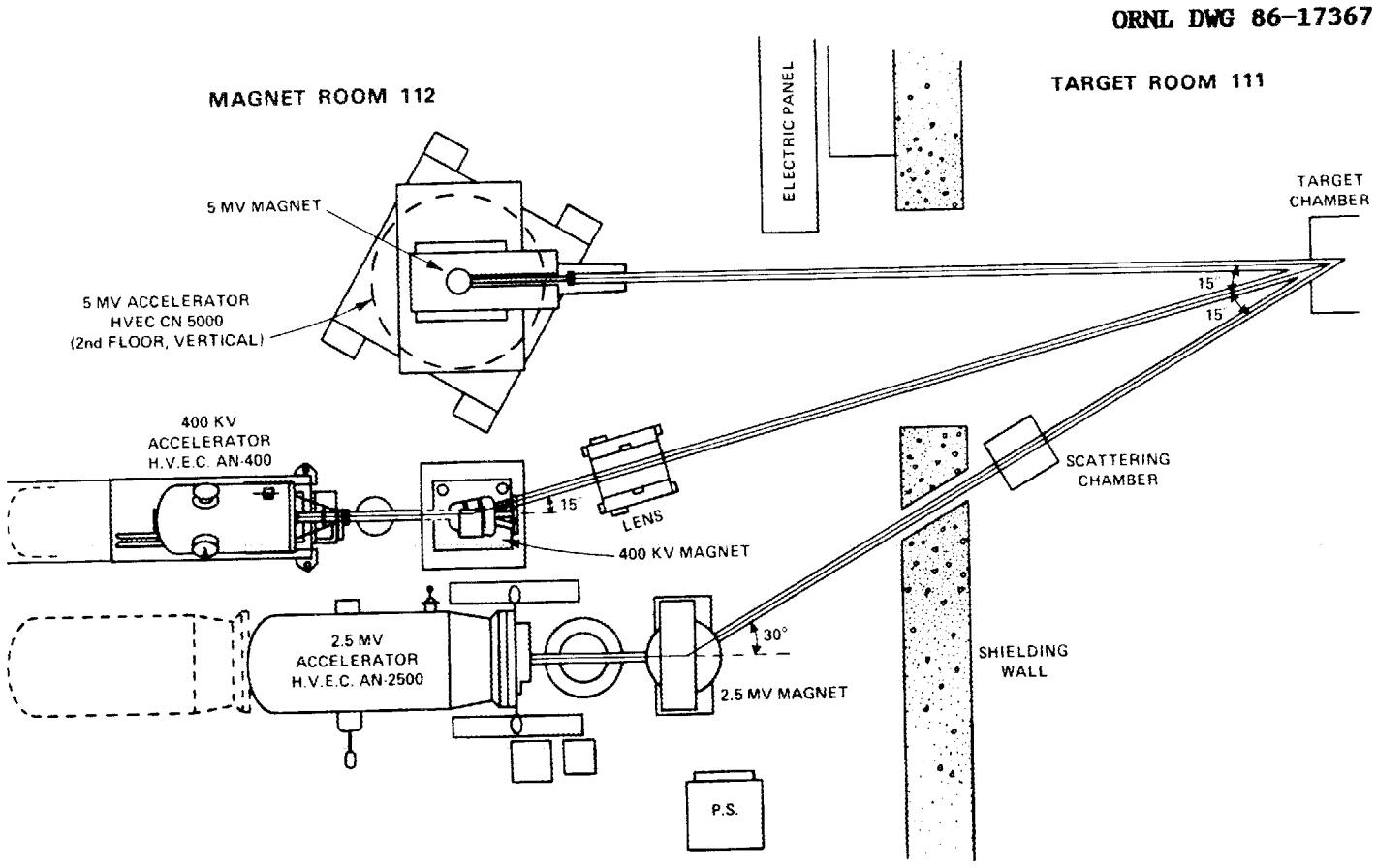

Fig. 2. A two-dimensional plan view of the beamlines in Fig. 1.

It is now operated primarily with a Model 910 Physicon ion source originally designed by Danfysik and based on the ion source research of Nielsen.[4] Although the Model 910 produces ample quantities of heavy metallic ions, its output of light ions, such as protons, is often not adequate. When high currents of light ions are needed, this source is replaced by a duoplasmatron source.[5] Details on the operation of the ion sources are given in Appendixes A and B.

The essential components of the terminal and beamline optics are shown schematically in Fig. 3. A more detailed and scaled drawing of the terminal only is shown in Fig. 4. At the source, carbon tetrachloride is brought into a quartz tube filled with metal powder. The metal (M) forms a metal halide and vaporizes near a hot filament. Electrons streaming from the filament to the anode ionize and dissociate the metal halide to form M^+ and Cl^+ ions.

Positive ions are accelerated out of the anode by the negatively charged extractor electrode. The ions are then focused by a three-barrel einzel lens into a Wien velocity filter (ExH mass analyzer) that is adjusted to allow only the metal ions to pass, thus reducing the total beam current and accelerator loading. The mass resolution is shown in Fig. 5. The metallic ions are refocused by a gap accelerating lens before entrance into the main accelerator tube. After acceleration to a few million electron volts, if the mass-energy product is greater than 60, the M^+ ions have to be stripped to charge state +2 in order to be analyzed by the 90° magnet. The stripping is done by directing the ions through a differentially pumped argon gas-filled tube. A summary of typical beam intensities at various points along the beamline is given in Table 1.

The metal ion beam bombards a target area of about 1 cm^2. It is desirable to irradiate such a surface as uniformly as possible with minimum loss of ion beam flux. Because of the high divergence of the beam at the control slits [(f) in Fig. 1] and the long path to the target chamber [(l) in Fig. 1], a special split field ring lens[6] [(i) in Fig. 1] was developed and mounted along the ion path. Assuming that the distribution of the ions in the beam is radially Gaussian, the function of the lens is to deflect the Gaussian tail region of the beam into the more central portion, which is itself unchanged by the zero field center of the lens. The

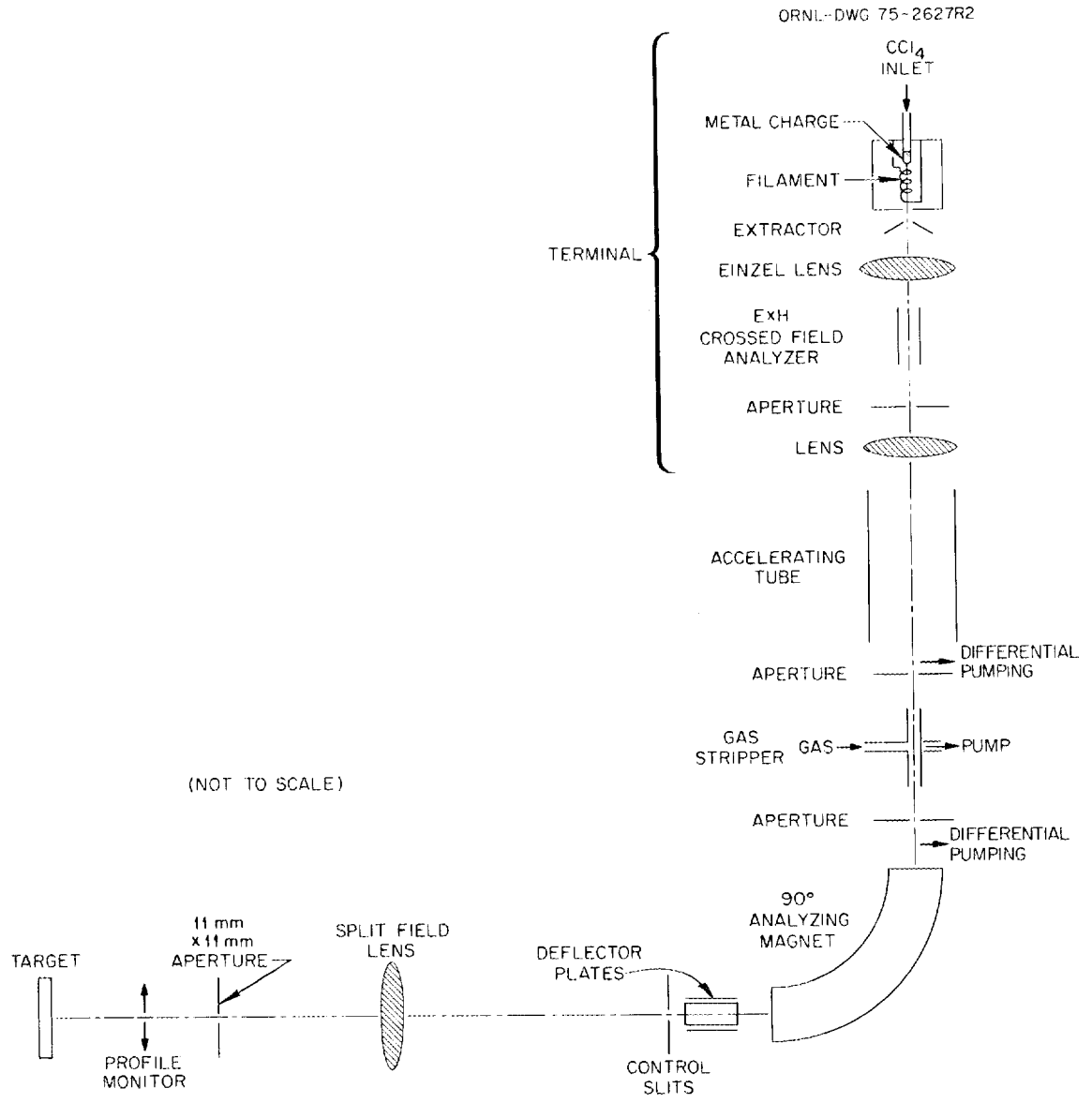

Fig. 3. Schematic drawing of the 5-MV accelerator beamline showing the respective components. The drawing is not to scale. Ions are produced in the terminal, accelerated, analyzed by the 90° magnet, and focused onto the target by the split field or "ring" lens.

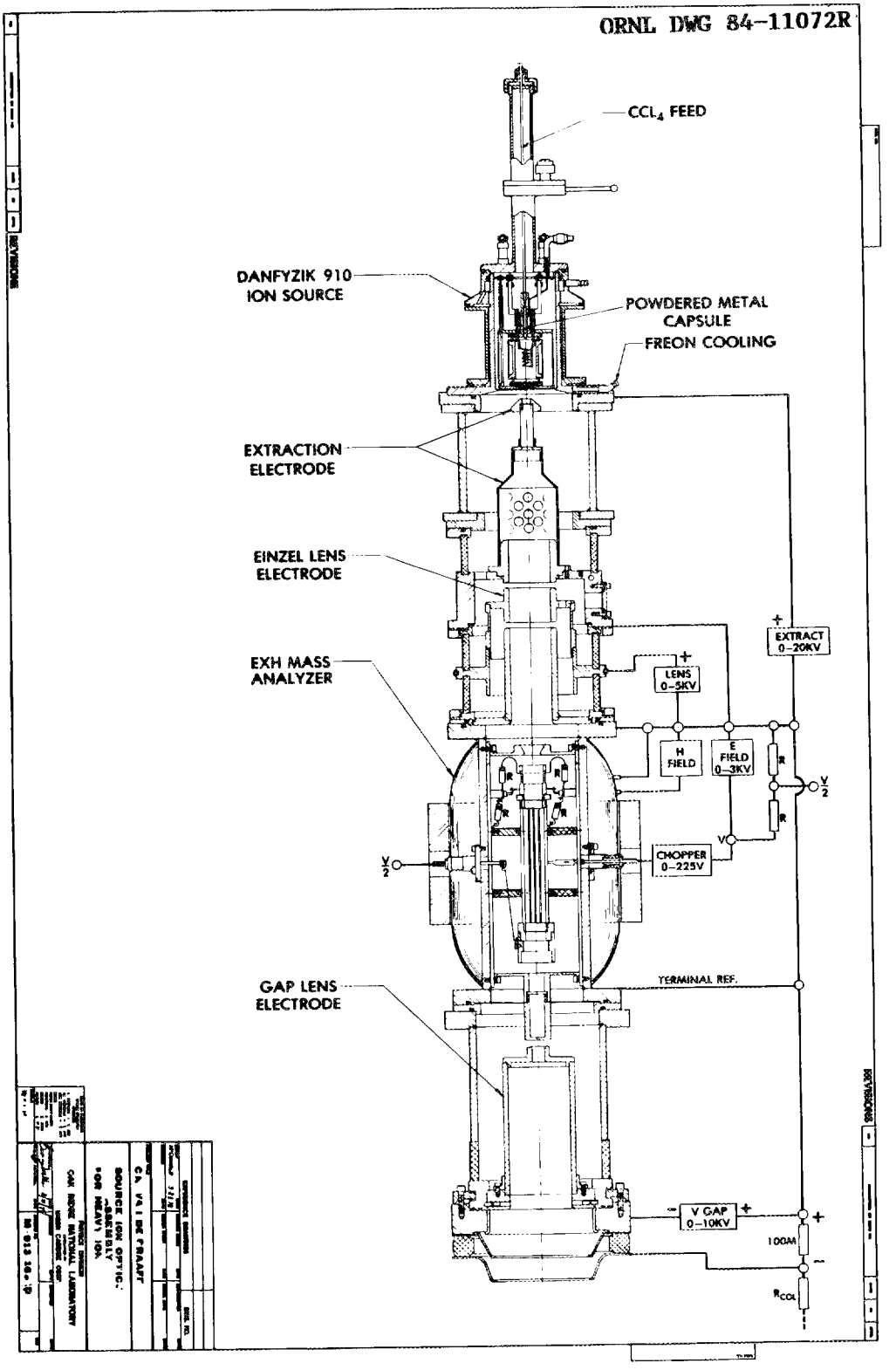

Fig. 4. Cross section of the heavy-ion source (Danfysik 910) and extraction system to which a fast switching circuit has been added in series with the electric field to permit the option of "chopping" the resulting ion beam before acceleration.

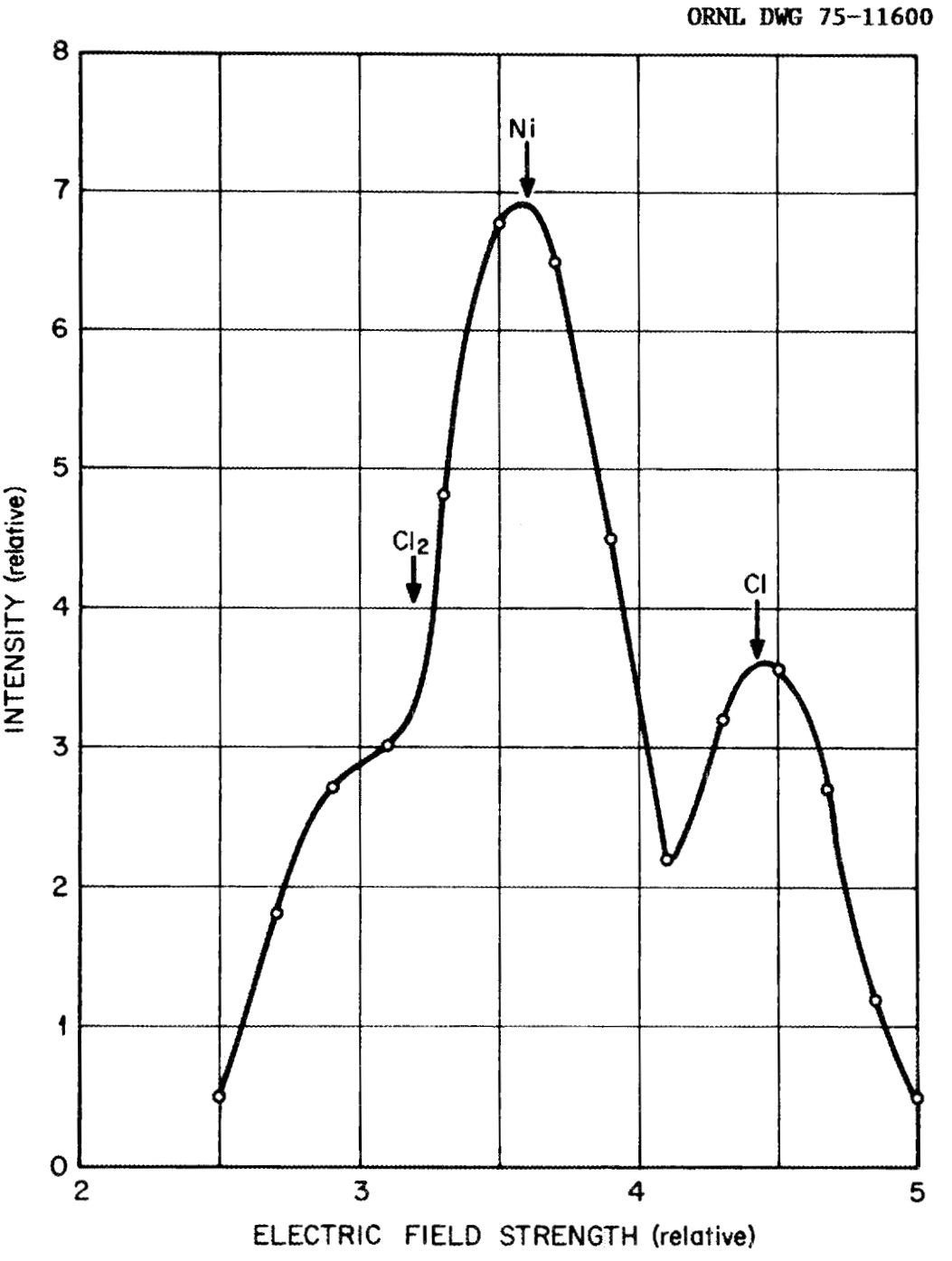

Fig. 5. Ion beam intensity measured (before the gas stripper) as a function of the electric field strength in the velocity selector located in the terminal. The arrows indicate the expected positions for Cl_2^+, Ni^+, and Cl^+.

Table 1. A summary of typical beam currents at various sites along the beam transport system

Location	Components	Intensities (μA)
Before stripper	Ni^+	~12
	Cl^+, Cl_2^+	~4, ~1
	C^+	Not seen
After stripper	Ni^+, Ni^{2+}, Ni^{3+}, -	~24 (total)
	Cl^+, Cl^{2+}, Cl^{3+}, -	~8 (total)
	C^+	Not seen
Control slits	Ni^{2+}, Ni^{3+}	5.2, 5.0
	Cl^{2+}, Cl^{3+}	1.3, 1.6
	2 MeV Cl^{2+} (from dissociation of Cl_2^+)	1.0
	C^+	<0.05
Target	Ni^{2+}	2.4

divergence of the beam is so modified that its cross-sectional area at the target is reduced and made more uniform in intensity. Details of the ion beam transport are given in Appendix A.

Beam chopping has also been added to the capabilities of the system. Magnetically actuated pivoting beam stops are used in conjunction with a dual binary programmable timer to allow a wide range of chopping or pulsing parameters. Presently, this range is variable and can be set as low as 0.1 s. Both beam-on and beam-off periods can be independently adjusted. The beams from both the 5-MV and the 400-kV machines can be chopped simultaneously. The beam stops are located about 80 cm upstream from the target chamber along the respective beamlines. High-frequency beam chopping, up to 0.1 MHz, has been realized by using a push-pull oscillator to control the voltage on the parallel plates of the ExH analyzer in Fig. 4. Further details of this technique can be found in ref. 7 and Appendix C.

2.3. THE 400-kV ACCELERATOR AND BEAMLINE

The type "AN" (50- to 400-kV) Van de Graaff, also built by HVEC, was initially used to implant alloys with helium in low concentrations to simulate helium generated by neutron transmutations in breeder reactor fuel cladding material or in fusion reactor first-wall material. The ion source for the AN is of the "RF" type, with a quartz bottle containing low-pressure gas surrounded by a radio-frequency exciter field to ionize the gas; typical light ions presently accelerated are H^+, He^+, B^+, CH_4^+, N^+, O^+, and F^+.

Beam uniformity over the target is in this case accomplished by beam expansion and collimation ahead of the target. The expansion takes place at the singlet quadrupole lens [(p) in Fig. 1], whereas the 1-cm^2 defining aperture is located downstream from the lens and near the target chamber.

When it is important to make the depth of light-ion implantation overlap the broad depth region of radiation damage caused by the heavy-ion beam, the AN 400 energy is varied continuously by cycling the terminal voltage from 200 to 400 kV. To maintain lateral beam uniformity as the energy is changed, the singlet quadrupole lens current is also cycled. The automatic control arrangement by which the beam energy is varied while maintaining a uniform intensity on target is shown in Fig. 6. The heart of the system is a variable frequency signal generator that provides the driving ramp signal for all controlled devices. Each power supply has a reference and a ramp signal so that the accelerator may be operated in a conventional mode (without ramping) or in a voltage-cycling manner.

2.4. THE 2500-kV ACCELERATOR AND BEAMLINE

The "AN" (200- to 2500-kV) Van de Graaff was recently built by HVEC and is similar in design to the AN 400, except that the RF source is larger and capable of delivering several hundred microamps of current. This accelerator is equipped for external control of three source-gas supplies. Although only gases such as H_2, He, BF_3, CH_4, N_2, and O_2, Ne, or Ar are presently used in this source, future development will include metals such as Mg and Al.[8]

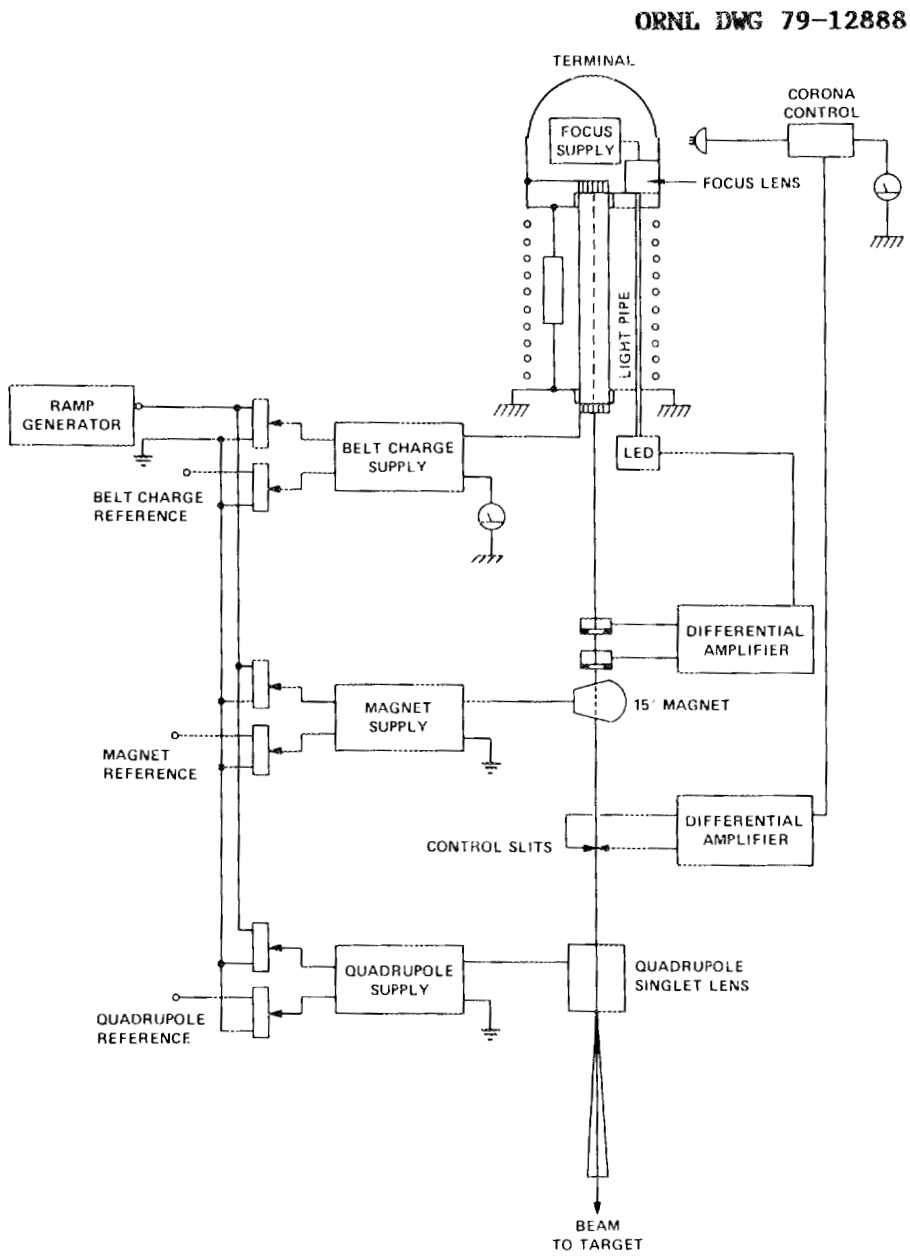

Fig. 6. Block diagram of the automatic variable-energy control of the 400-kV Van de Graaff. The system is initiated by varying the analyzing magnet current and triggering the stabilizing amplifier to change the terminal voltage. Simultaneously, the current in the quadrupole singlet is cycled to maintain a fixed ion-beam focal point during the terminal voltage cycle.

In order to increase the uniformity of the ion beam over targets as large as a square centimeter, a wobbling technique is sometimes used. This consists of a set of magnetic steering coils [(r) in Fig. 1]. The current to these coils is driven by a programmable power supply that is, in turn, governed by a function generator. One power supply and generator is needed for each wobbling direction.

3. TARGET CHAMBERS

3.1. TRIPLE-BEAM CHAMBER

3.1.1. Chamber Construction

The triple-beam chamber is geometrically located at the intersection of the three accelerator beamlines in Fig. 1 and is shown in Fig. 7. The body is constructed from intersecting stainless steel tubes, the outer ends of which terminate in standard ultrahigh vacuum (copper gasket) flanges. The target assembly has six individual target/heater modules in a row, a large bellows which permits 230 mm of linear motion along the axis of the row, and all power and instrumentation feedthroughs. A precision machine-tool bed attached to the chamber body is used to manually align any desired target with the common intersection point of the three charged-particle beams. The beams enter the chamber by separate ports with 15° angles between them. Other ports at the same angle relative to the heavy-ion beam permit illumination and visual observation of the specimens during bombardment.

Clean ultrahigh vacuum is provided by a 1000-ls^{-1} cryopump together with two liquid-nitrogen sorption pumps that are used for initial pump-down. The cryopump, attached to the chamber through a large-diameter gate valve and an elbow coupling to minimize the radiant thermal load from the specimen heaters, is used below about 2×10^{-3} torr. If no specimens are being heated, the chamber can be pumped to a base pressure as low as 7×10^{-9} torr. Actual bombardment of specimens at 600°C is generally conducted with a vacuum in the low 10^{-7} to high 10^{-6} torr range. Both a nude ionization gage and an intermediate-range Varian millitorr gage are used to monitor the pressure, whereas a Varian

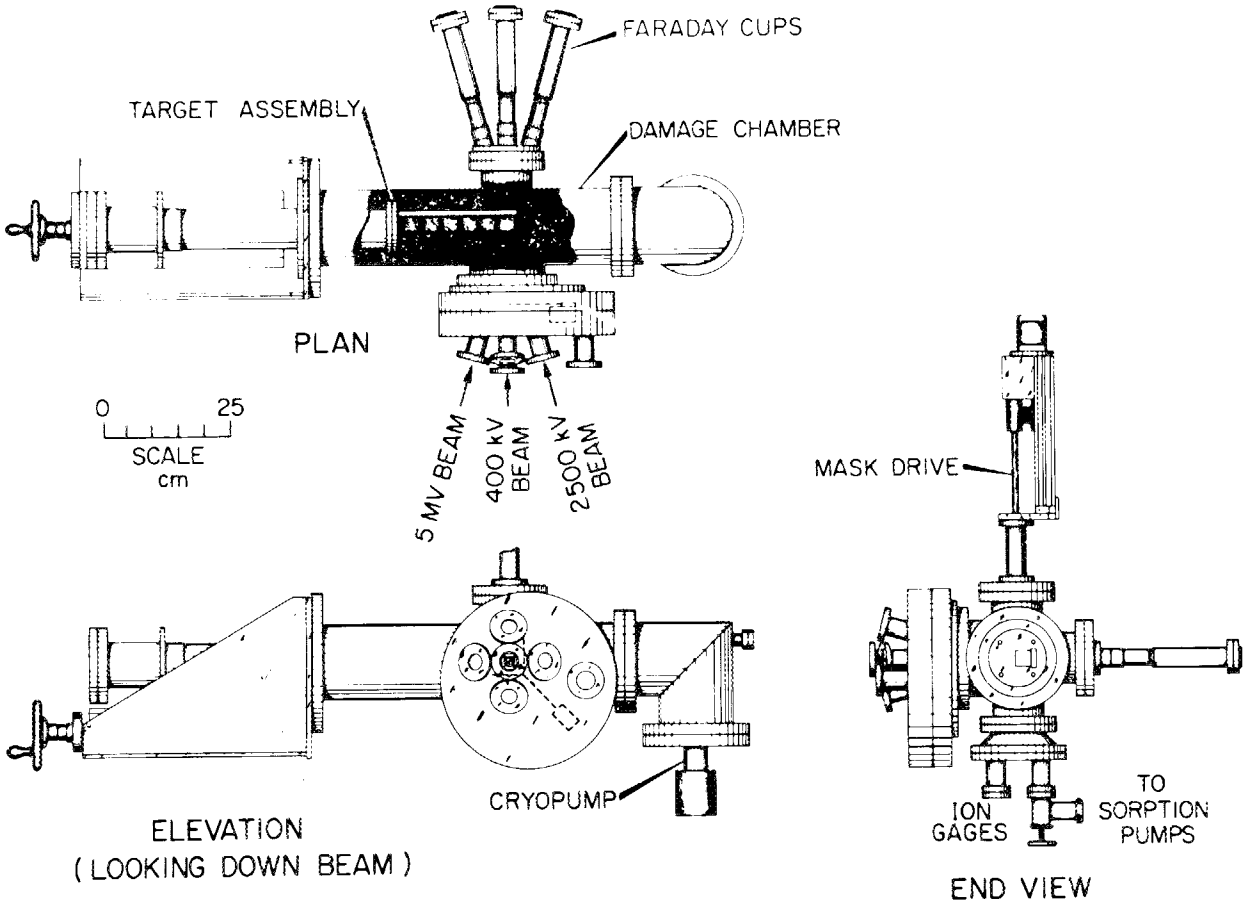

Fig. 7. Layout of the triple-beam radiation damage target chamber showing the three ports through which the beams pass before striking the target.

quadrupole residual gas analyzer (RGA) is available to evaluate the composition of the remaining atmosphere. A typical spectrum from the RGA is shown in Fig. 8. (The primary peaks in such a spectrum are readily identifiable in the figure.) The water vapor pressure is high because of the strong dipole moment of the H_2O molecule which makes it resistant to pumping. The dissociation of H_2O in the analyzer gives rise to OH and H peaks. The H_2 and CO_2 peaks are assumed to be contaminants of the stainless steel in the chamber itself. The argon peak is from the argon gas stripper upstream from the chamber.

Built into each target assembly is a resistance-heating loop and a water-cooling channel. Heating to ≈100°C hastens out-gassing just after pumpdown, whereas the water line hastens the necessary cooling of specimens and heaters to ambient temperature before being exposed to air. A more complete description of the system can be found in ref. 9.

3.1.2. Faraday Cups

The triple-beam chamber was primarily designed to irradiate simultaneously nine transmission electron microscopy (TEM) specimens spanning a total area of 1 cm^2. For this reason, it is important to know the beam flux level at the sites of the nine samples.

An array of nine miniature Faraday cups (Fig. 9) on the 5-MV line is used to measure the beam current just in front of the position in which the specimens are located. These cups have an aperture plate in front to collimate the beam and reduce secondary electron interference. They have a length/diameter ratio of 4.45 and an entrance aperature diameter of 2.01 mm. The cups are symmetrically located in the beam on 3.43-mm centers. Similar cup assemblies on the 0.4- and 2.5-MV lines have five individual cups (with an entrance aperature diameter of 2.26 mm) located at the corners and in the center of the irradiated area; the four remaining currents corresponding to the remaining TEM disks in the target are estimated by interpolation. A bellows-sealed pneumatic activator is used to position the cups in the beams directly in front of the target. This device is activated under computer control, typically every 10 min of irradiation. After the cup assembly has been inserted for about 20 s and readings have been taken, the results are printed for each cup on the three beamlines. An example of typical numbers in arbitrary units is

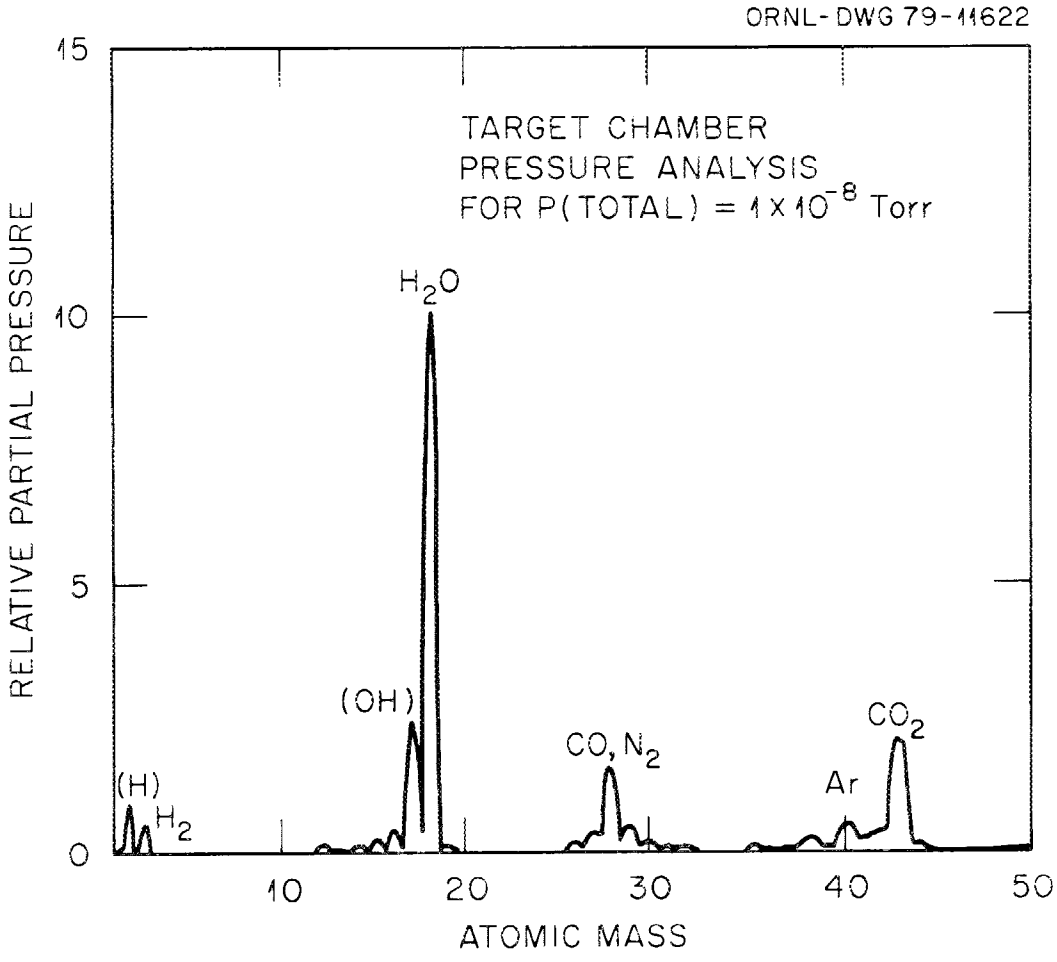

Fig. 8. Residual gas analyzer spectrum of the target chamber under typical vacuum conditions of 1×10^{-8} torr.

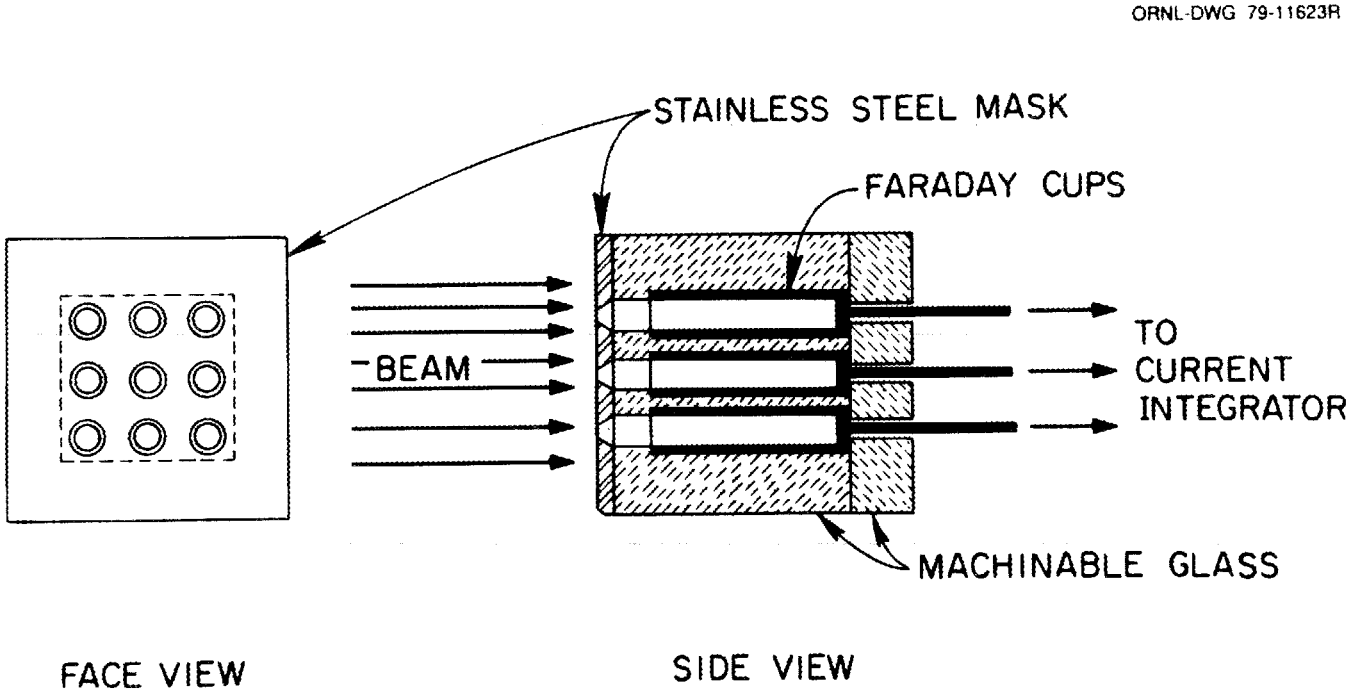

Fig. 9. Two schematic views of the nine miniature Faraday cup arrays used to asssess the true x-y beam intensity on target.

given in Table 2. The parameters at the top are selected at the beginning of the run. The beam currents at the middle of the table are used by the accelerator operator to make final tuning adjustments before the run begins. The accumulated dose (dpa) for all beams and the concentrations (appm) for each beam are printed out at regular intervals during a run and are shown at the bottom of Table 2.
of Table 2.

3.1.3. Electron Gun Heaters

Figure 10 is a view of a target assembly with each of the six specimen/holder heater modules in progressive stages of assembly. The heaters, located behind the targets, are dispenser cathode triode-type electron gun assemblies. The support structures around the guns were machined from Macor glass-ceramic material. The electron guns operate with the cathode at 600 to 800 V negative to ground drawing ~10 mA, whereas the specimen assembly at ground potential serves as the anode. Very sensitive control is afforded by varying the potential on the fine mesh grid from about 0 to -1 V with respect to the cathode. The cathode is heated by an internal filament that requires about 1.5 to 2.0 A at 10 to 12 V. Since the grid and filament are operated relative to the negative cathode potential, their power supplies must be electrically isolated from ground (via an isolation transformer) and physically enclosed within a Plexiglas cage. Across this potential difference, control is accomplished by a pair of voltage/frequency optical isolation couplers. The heaters can bring a target temperature up to about 825°C.

3.1.4. Specimen Holders

The specimen holders mount directly in front of the electron gun heaters; there is a space of about 0.8 mm between the electron gun grid and the lower portion of the specimen holder (thermalizer block). The two parts of the specimen holder, the thermalizer block and the face plate, clamp the specimens between them. Both specimen holder parts are fabricated from Kulite-112 machinable tungsten alloy to reduce problems of bonding with most specimen materials. A crushable ring of annealed platinum wire, 0.1 to 0.2 mm thick, is placed between the face plate and

Table 2. Format and test run values for all information printed out during a triple ion beam run. The parameters at the top are selected at the beginning of the run. The beam currents at the middle of the table are used by the accelerator operator to make final tuning adjustment before the run begins. The accumulated dose (dpa) for all beams and concentrations (appm) for each beam are printed out at regular intervals during a run and shown at bottom of the table.

```
        ZINKEL----AL20J
        RUN  123            DATE    7/  11/  88          STATION    4

PARAMETER OPTIONS CHOSEN ARE
(11,12,13) MICROCOUL/DPA FOR THE 5MV,2.5MV,400KV BEAMS=  330  1000  8000
(2) COULOMB/PULSE =  0.000000009100
(3) COUNTING TIME PER CUP (SEC.) =      2.00
(4) STD. DEV. IMPLANTED 2.5MEV ION DIS. =      0.10
(6) ATOMIC DENSITY (10^22) =     11.70
(7) STD. DEVIATION OF IMPLANTED LIGHT ION DIS. =      0.22
(8) DURATION BETWEEN CUP READINGS (SEC.) =     60.00
(9) HELIUM CUP CALIBRATION FACTOR =      0.50
(10) 2.5 MEV CUP CALIBRATION FACTOR =      0.50
    400 KV ENERGY=  300  ION MASS=   4
    2.5 MV ION ENERGY= 1400  ION MASS=  16
    5 MV ION ENERGY=    2  ION MASS=  27
RUN TERMINATION CONTROLLED BY TOTAL DPA DOSE FROM ALL IONS AT    40 DPA

STARTING TIME= 1259.5

00000  INITIAL CUP READINGS BEFORE RUN STARTS  00000

                    BEAM CURRENTS (*10-9 AMPS)
        5 MV CUP ARRAY                400 KV CUP ARRAY                2.5 MV CUP ARRAY
      99.30     96.75     96.70      99.25     97.55     96.70      99.30     97.55     96.70
      96.65     96.70     96.70      97.55     96.70     96.68      97.55     96.65     96.67
      96.70     96.70    101.65      96.70     96.68     96.65      96.70     96.67     96.65

      5 MV DEEP CUP=     0          400 KV DEEP CUP=     0          2.5 MV DEEP CUP=     0
      CALCULATED TOTAL=  3039       CALCULATED TOTAL=  2931         CALCULATED TOTAL=  2926
      TOTAL DPA/HOUR=    43         APPM(400 KV)/HOUR=  8387        APPM(2.5 MV)/HOUR= 18553        APPM(400 KV)/DPA=   195
      %PROFILE ERROR(5 MV) =     2  %PROFILE ERROR(400 KV)=     1   %PROFILE ERROR(2.5 MV)=     1

                    ********** ACCUMULATED VALUES AND CUP CURRENT (E-9 AMPS) **********

 TIME---------TOTAL DPA----------------5MV APPM----------------5MV CURRENT----------------400KV APPM----------------400KV CURRENT----------------2.5MV APPM----------------2.5MV CURRENT----------TEMP.+C----
 13: 2    0.7    0.7    0.7      401.5  391.2  391.0      99.3   96.8   96.7      145.1  142.6  141.3      99.3   97.6   96.7      321.1  315.5  312.7      99.3   97.6   96.7
          0.7    0.7    0.7      390.9  391.0  391.0      96.7   96.7   96.7      142.6  141.4  141.3      97.6   96.7   96.7      315.5  312.7  312.7      97.5   96.7   96.7       24.0
          0.7    0.7    0.7      391.0  391.0  410.9      96.7   96.7  101.6      141.4  141.4  141.3      96.7   96.7   96.7      312.7  312.7  312.7      96.7   96.7   96.7

          AVG DPA(TOTAL)=    1    AVG APPM(5MV)=   394    CAL. TOTAL(5MV)=  3014    AVG APPM(400KV)=   142   CAL. TOTAL(400KV)=  2926    AVG APPM(2.5MV)=   314    CAL. TOTAL(2.5MV)=  2926        ETA:  1414
                                   ION/CM2(10^15)=   1    %DEVIATION(5MV)=     2    IONS/CM2(10^15)=     1   %DEVIATION(400KV)=     1    IONS/CM2(10^15)=     1    %DEVIATION(2.5MV)=     1

 13: 4    1.6    1.6    1.6      914.8  892.3  891.1      99.3   96.8   96.8      290.3  285.3  282.7      99.3   97.6   96.7      642.1  631.0  625.5      99.3   97.6   96.7
          1.6    1.6    1.6      891.8  890.9  890.9      96.7   96.7   96.7      285.3  282.8  282.7      97.6   96.7   96.7      630.5  625.4  625.4      97.3   96.7   96.7       24.0
          1.6    1.6    1.6      890.9  890.9  930.6      96.7   96.7  101.6      282.7  282.7  282.6      96.7   96.7   96.7      624.0  624.9  625.3      95.9   96.4   96.7

          AVG DPA(TOTAL)=    2    AVG APPM(5MV)=   898    CAL. TOTAL(5MV)=  3014    AVG APPM(400KV)=   284   CAL. TOTAL(400KV)=  2926    AVG APPM(2.5MV)=   628    CAL. TOTAL(2.5MV)=  2921        ETA:  1415
                                   ION/CM2(10^15)=   3    %DEVIATION(5MV)=     2    IONS/CM2(10^15)=     2   %DEVIATION(400KV)=     1    IONS/CM2(10^15)=     2    %DEVIATION(2.5MV)=     1
```

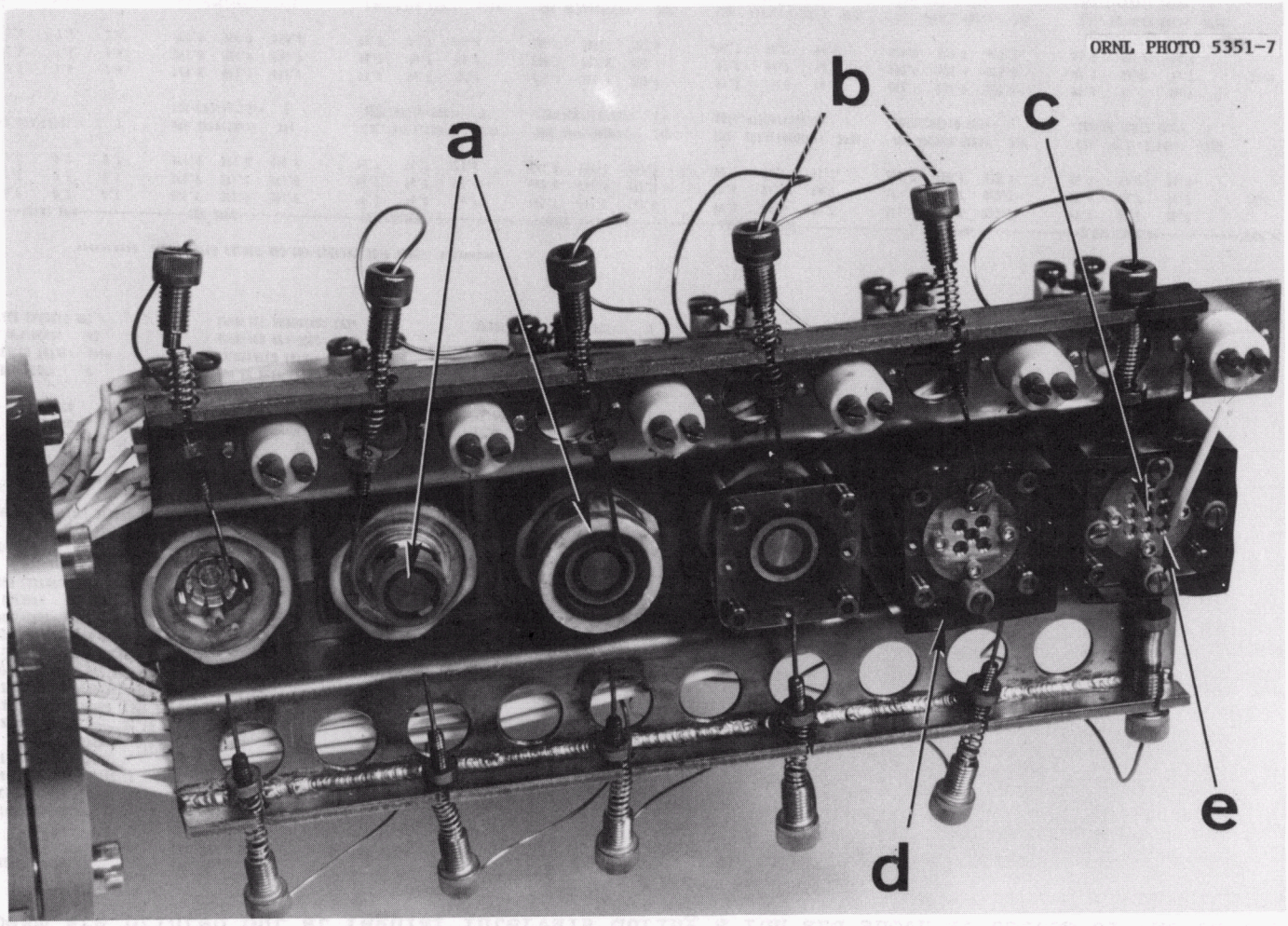

Fig. 10. Detailed view of the target assembly showing from left to right the six heater stations in progressive stages of assembly: (*a*) electron guns; (*b*) spring-loaded thermalizer block thermocouples; (*c*) nine-disk specimen holder; (*d*) tantalum heat shield; and (*e*) specimen thermocouple.

the specimen front surface to accommodate small specimen-to-specimen variations in thickness. A mask is available to shield selected specimens during part of a bombardment interval. In this configuration, large differences in fluence can be applied to individual specimens. The TEM specimen loading procedure is given in the Appendix D.

3.1.5. Temperature Control

Temperature control begins with the signal from either of two 1-mm-diam sheathed Chromel-P-Alumel thermocouples spring-loaded into 6-mm-deep holes in the edge of each thermalizer block. A third thermocouple output is available at each station for measuring the specimen surface temperature, using pairs of 0.13-mm-diam Chromel-P-Alumel wires spot welded near the periphery of a dummy specimen. All of these signals are led through a switching panel that permits any of the three to be used for control; any one may also be displayed on a room-temperature-compensated digital indicator. Temperature control is effected by means of a strip-chart recorder with current-adjusted type controllers; the control signal is fed back (via optical isolation) to the electron gun grid potential. The result is control, which is both rapid in response and stable. With an electron gun that has been "conditioned" since its last air exposure, a specimen holder starting at ambient temperature can be raised to and held at 700°C in <5 min, and any such irradiation temperature can be maintained within ~ ±1°C for at least several hours. With one specimen temperature measured directly by the thermocouple, the others (up to eight) are measured relative to the first by means of an infrared pyrometer that can be sighted on each individual specimen.

3.2. STRESSED-SPECIMEN CHAMBER

The stressed-specimen chamber [(m) in Fig. 1], located immediately downstream from the triple-beam damage chamber, is intended to generate through-thickness radiation damage in 40-μm-thick (0.0015-in.) ribbon specimens using a 4-MeV proton beam from the 5-MV Van de Graaff accelerator. In addition to providing the important parameter of a chosen

static tensile load during irradiation, the resulting quasi-bulk irradiated volumes are amenable to a variety of postirradiation characterizations, including thin-specimen tensile tests, nano-indentation hardness studies, fractography, and electron microscopy.

The layout of chamber components is depicted in Figs. 11 through 13. The ribbon specimen, 3 mm wide and from 125 to 280 mm (5 to 11 in.) long, is installed by means of upper and lower grips with internal wedge-holding into a load train that ends in a weight pan (weighing 100 g empty). Weights to achieve any desired static stress can be added directly through the lower port, whereas multiple locations (spaced 25 mm apart) on the ribbon can be moved into beam position using the upper linear motion drive.

Temperature control of the bombarded region of the ribbon is provided by a combination of beam heating, electrical heating, and forced-draft helium gas cooling. The very substantial heat input from the proton beam and sensitivity to beam fluctuations require a temperature control system that is both high capacity and fast acting. Current passing through the chamber and through the specimen augments beam heating and is regulated to control the operating temperature of the specimen. An infrared pyrometer acts as a feedback element that controls a phase-angle-fired silicon-controlled rectifier power supply via a Leeds and Northrup temperature controller. The chamber is operated with an internal atmosphere of about 0.016 MPa (120 torr) high-purity helium, isolated from the beamline vacuum by a 2.5-μm-thick Havar alloy foil window. The bombarded region of the specimen is situated in a cut-out notch of a channel, edge-on to a fast-flowing stream of helium. Additional jets of helium are directed at the front surface of the specimen above and below the beam centerline. There are also jets onto the foil window. Gold-plated posts (the inner pair of posts seen in the close-up view of Fig. 13) contain the specimen front-surface jets and also permit direct electrical current heating of the central 20 mm of specimen, largely reducing temperature fluctuations during irradiations.

The bombarded region is 3 mm (the ribbon width) by about 4.5 mm high. The desired temperature is currently attained only in the central 2-mm vertical portion. The temperature is monitored by an infrared pyrometer

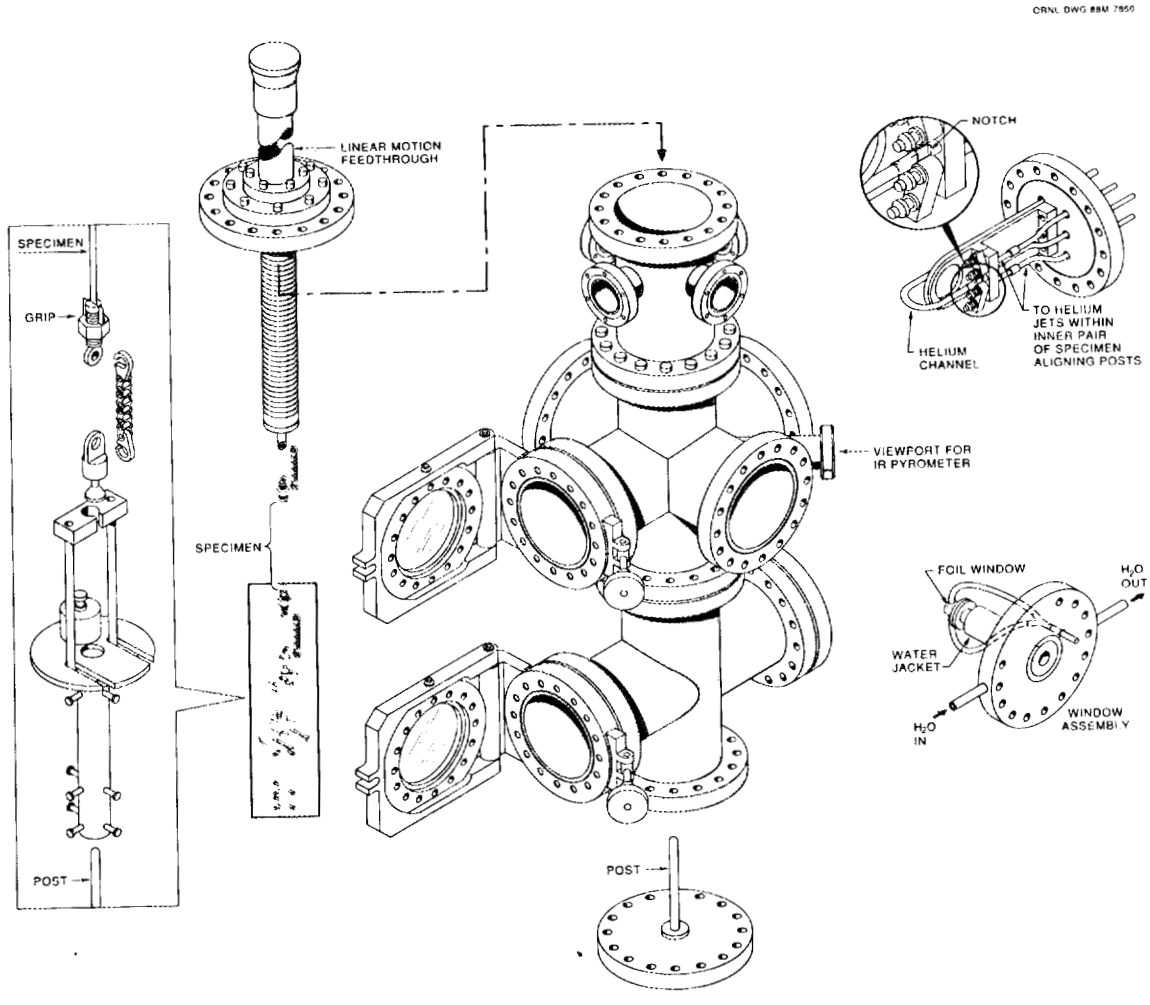

Fig. 11. Assembly view of the stressed-specimen chamber. A central region, about 4 mm high, of the 3-mm-wide by 300-mm-long ribbon specimen is bombarded by a beam of 4-MeV protons.

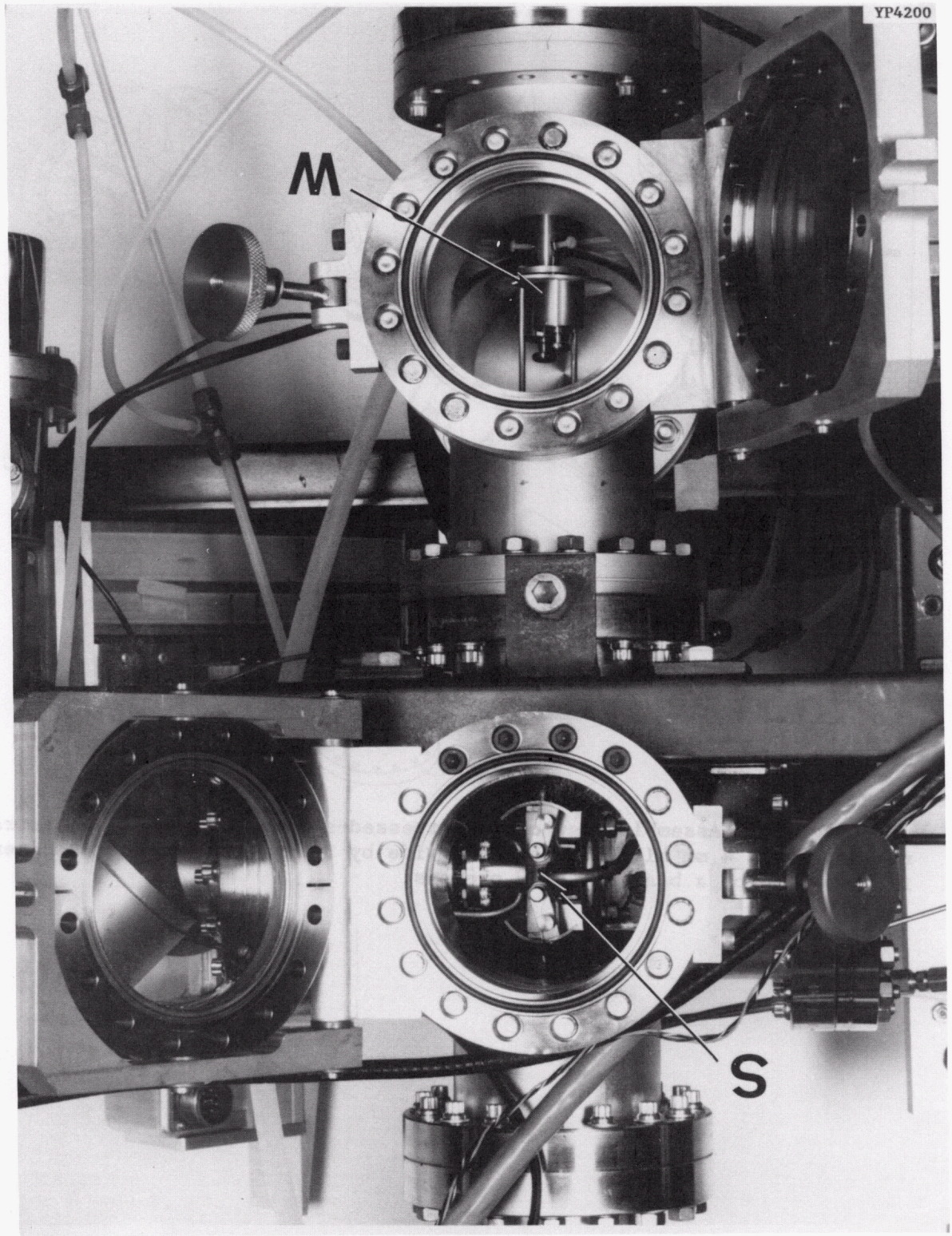

Fig. 12. Stressed specimen chamber showing the relative positions of the vertical ribbon (S) and the weights (W).

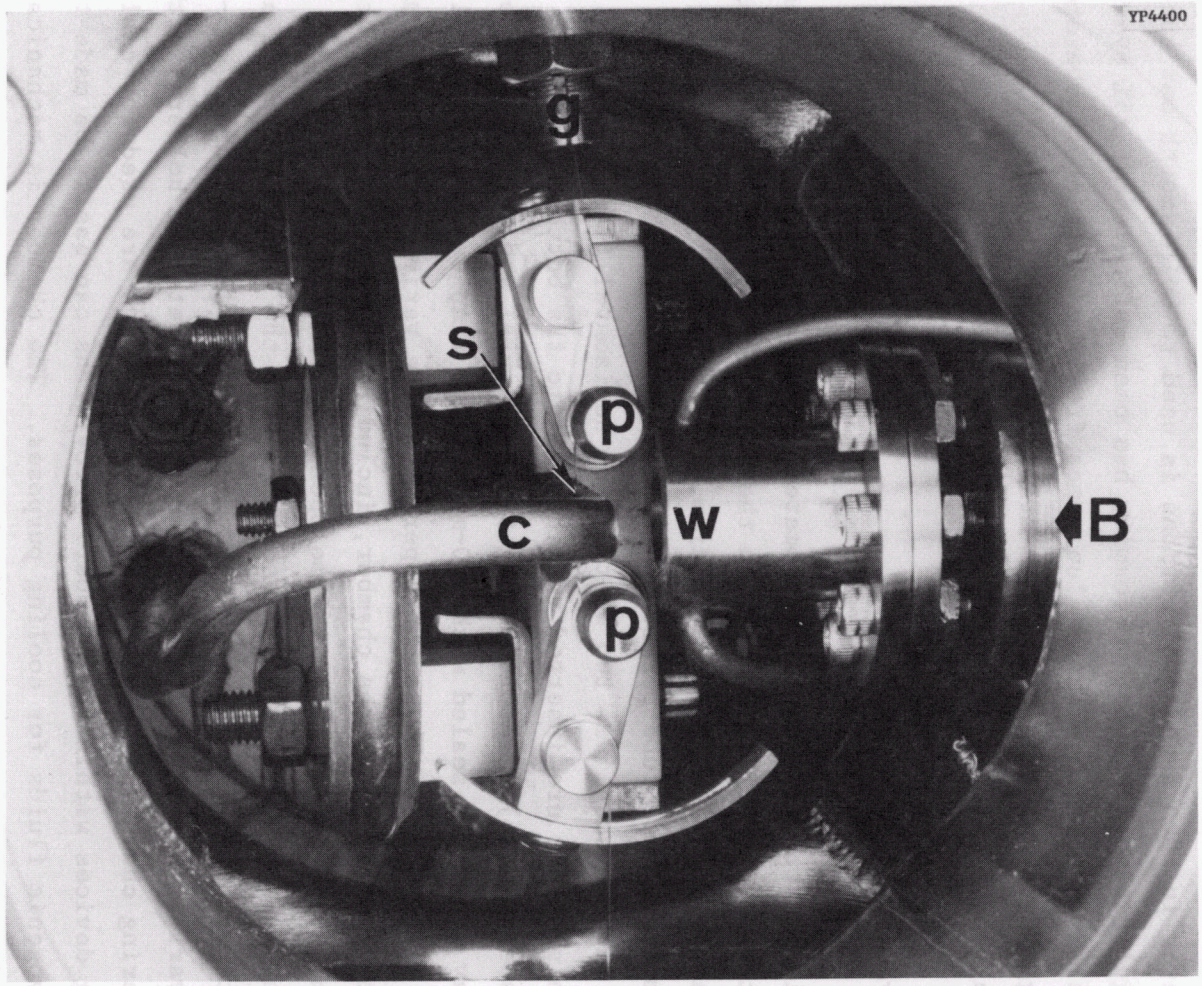

Fig. 13. Target region of the ribbon specimen showing the window (w), gold-plated support posts (p), the specimen grip (g), the specimen (s), and the helium gas channel (c). The direction of the ion beam (B) is also shown.

whose output can also be fed back to regulate the electrical specimen heating current. Day-long irradiations with proton beam currents of 7 to 8 μA (≈35 μA/cm^2) have generated depth-averaged damage levels of 0.2 dpa (such currents can raise the target to 450 to 500°C by beam heating alone). Wobbling the beam at 10 Hz at an amplitude of about one-third beam diameter in both X and Y directions is used to help smooth out spatial irregularities. Fluence uniformity has been estimated at ±5% over the central 2-mm portion. This value comes from immediate postbombardment autoradiography of Ni-8% Si specimens utilizing the ^{64}Ni (p,n) ^{64}Cu activation, which has a half-life of 12.7 h.

3.3. ION-SCATTERING CHAMBER

The ion-scattering chamber is located upstream from the triple-beam chamber at position (t) in Fig. 1, on the AN 2500 beamline. The housing of the chamber consists of a 200-mm-diam, six-way cross. Sections of the 150-mm-diam drift tube permit an ion beam to enter and exit the ultrahigh vacuum vessel via two of the four horizontal flange openings. Sample manipulators are inserted vertically into the bottom chamber opening (see Fig. 14). The remaining two horizontal and top openings of the six-way cross are sealed with 200-mm Conflat flanges having several 70-mm and 34-mm ports. These ports permit a wide variety of high-vacuum flanges to be attached to the chamber, including electrical, linear/rotary motion, and fluid feedthroughs. Some openings are covered with transparent viewports for visual inspection from the exterior; others are fitted with vacuum gages. Some Conflat flanges provide mechanical support for various apparatus (e.g., surface-barrier detector holders) within the scattering chamber. Instrumentation feedthroughs are used for cabling to sensing devices within the chamber. Provisions can easily be made to supply cryogenic fluids for cooling purposes. The chamber is mechanically supported from above by brackets attached to lengths of I-beam steel parallel to the beamline. Bellows on the beamline and screw adjustments on the attachment brackets permit vertical and lateral adjustment of the entire scattering chamber.

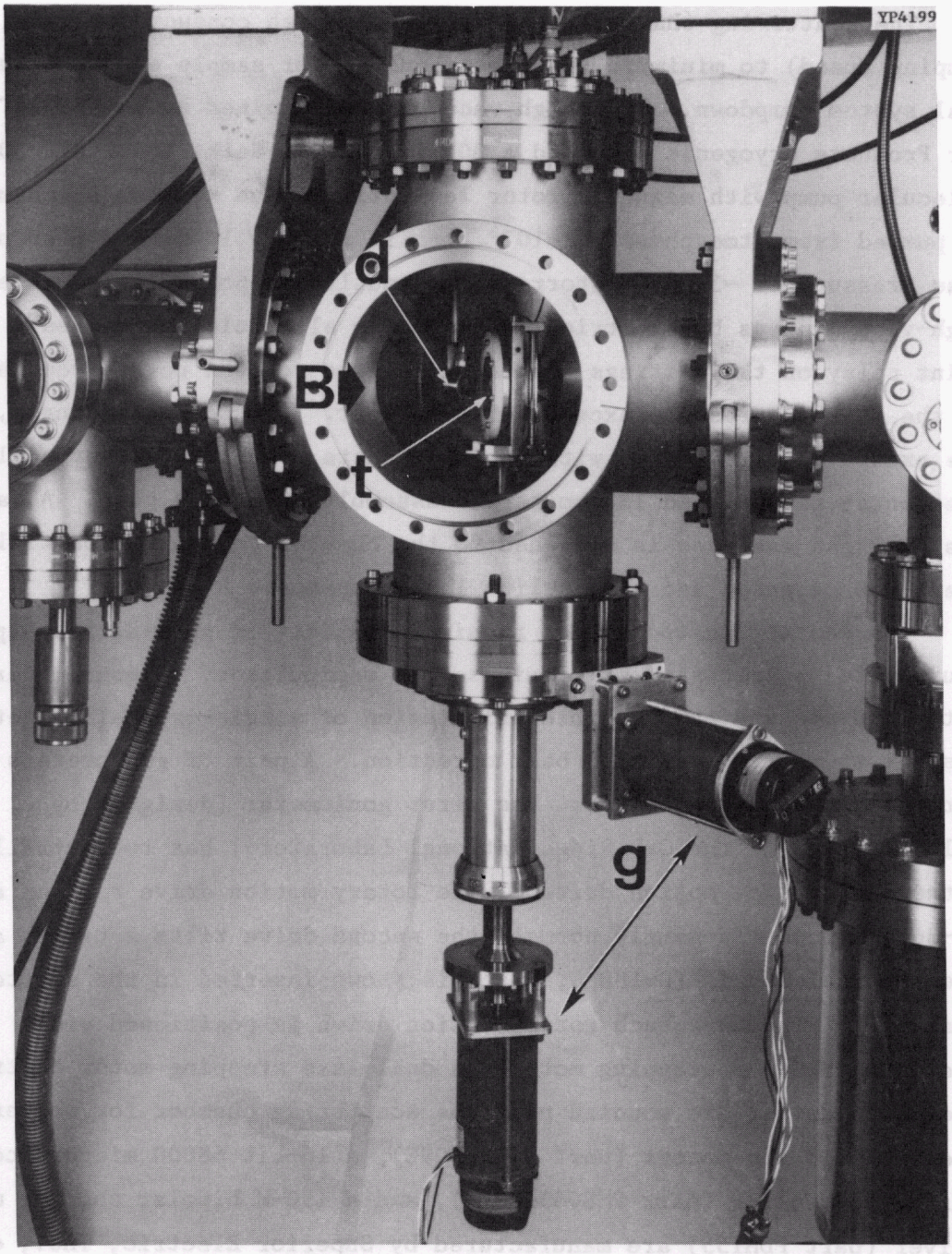

Fig. 14. Side view of the ion-scattering chamber with the 2-axis goniometer in position. B is the ion beam direction, t is the target support, d is the ion-scattering detector, and g denotes goniometer motors.

The scattering chamber is designed with high conductance (i.e., high pumping speed) to minimize the time required for sample exchange and initial system pumpdown. Ultrahigh vacuum is maintained by a 1000-ls^{-1} Air Products cryogenic pump and a 300-ls^{-1} Seiko-Seiki Model STP-300 turbo molecular pump with magnetic rotor levitation. The scattering chamber can be pumped from atmosphere to ~10^{-6} torr in roughly 10 min with an ultimate base pressure of ~3×10^{-8} torr. A six-outlet ac power strip protects high-vacuum pumps by electrically servicing all isolation valves. A set-point relay on the Hastings thermocouple gage removes power from the strip if the chamber pressure exceeds ~5 millitorr. All Conflat flanges, with one exception, are sealed with copper gaskets. A Viton gasket seals the frequently reassembled 150-mm target assembly insertion port. A Varian residual gas analyzer is attached to the chamber to monitor partial pressures of gases and as a helium leak detector.

Ion-scattering techniques require a variety of specialized support equipment. A precision multiaxis sample manipulator, or goniometer, permits accurate and reproducible orientation of single-crystal targets with respect to the incident ion beam direction. A pair of goniometers are currently available for use. The first goniometer (designed by Bill Appleton of the Oak Ridge National Laboratory) has two mutually orthogonal rotary motion drives. One rotary motion drive rotates a target (0–360°) about the sample normal; the second drive tilts a target around the vertical Z-axis (0–180°), which is shown inserted in the scattering chamber in Fig. 14. Each rotary motion drive is positioned via a precision SLO-SYN stepping motor. A dual-axis stepping motor controller and motor driver are mounted near the scattering chamber for convenience. The two stepping motors (part M063FD09E), a 16-bit 68000 microprocessor-guided controller (part PMS085-C2AR), and a 150-W bipolar chopper motor driver (part PDM155) are manufactured by Superior Electric, Inc., of Bristol, Connecticut. The controller has a RS-232C interface for communications with a remote dumb terminal in the shielded accelerator control room. Each motor can be driven individually from a keypad on the front panel of the controller or by a string of motion commands stored in a nonvolatile E^2PROM memory. The E^2PROM memory can be segmented for the storage of multiple operations (or subroutines) and can be programmed from

either the front panel of the controller or the remote terminal. The user may select absolute or incremental modes of motion, motor speeds, move distances, and acceleration/deceleration rates. Each motion stage is calibrated to be driven in 0.005° increments in the full-step mode of stepping motor movement with a motion precision of ±0.02°. Manual manipulation with knurled knobs on the shaft ends is possible, provided the controller power is off. When powered and idle, both windings on each stepping motor are energized to inhibit unintentional motion. Signals from a potentiometer readout on each rotary drive determine the angular position of the sample normal. The gearing (number of teeth per inch) between the rotary motion drives and the moveable target stage calibrates the counters to read in a standard unit of measure of 0.01°. Sliding Viton O-ring seals on the rotary motion drive shafts preserve the vacuum integrity of the goniometer chamber. Samples are fastened to a target assembly mechanically attached to the goniometer motion stages. A target is carefully positioned at the common rotational center of the two rotation axes. The entire sample head can be translated vertically over a 100-mm travel distance. This enables the target assembly to be retracted from the path of the ions for routing the ion beam into the downstream damage chamber.

A target assembly, as shown in Fig. 15, holds samples for analyses and ensures proper charge collection for ion fluence measurement. The central region of the target assembly is isolated from ground to serve as a Faraday cup for monitoring the ion beam current striking the target. A positive bias is applied to the target assembly to suppress the ejection of most of the secondary electrons produced during ion bombardment. Sample disks or targets as large as 20 mm in diameter can be routinely handled. The most frequently used target mask has either a 2.5- or 4.5-mm central opening for 3- and 5-mm disk, respectively. Satellite 2.5-mm apertures in the mask allow the insertion of an auxiliary reference standard or multiple samples for routine analyses. A metal mask covering the sample is especially important for charge collection in the examination of ceramic or nonconducting targets. A typical metal mask is constructed of 1-mm aluminum with a thin evaporated coating of gold. Ions scattered from gold nuclei appear prominently in backscattered energy

YP5063

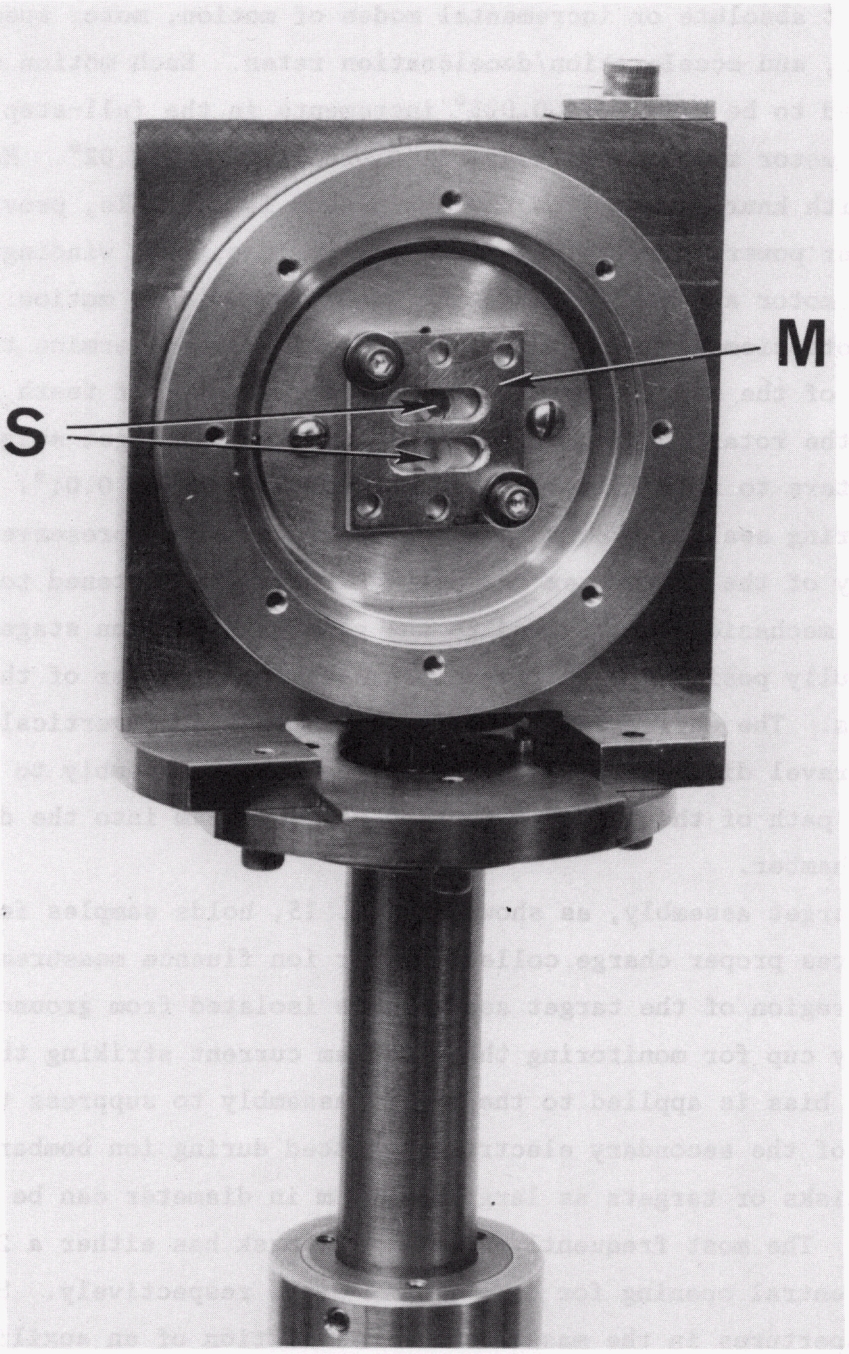

Fig. 15. Close-up view of the target assembly for forward-reaction scattering analysis in the ion-scattering chamber. Target specimens are shown by S, whereas the gold-plated target mask is shown by M.

spectra because of scattering kinematics. This serves as an aid for positioning the ion beam on the target surface. Thicker masks generally have an area recessed on the sample mounting side or are slotted to ensure that the aperture lip does not shadow the detector from scattered particles or reaction products departing the surface. The mask shown in Fig. 15 holds two 5-mm disks in slotted openings.

Channeling analyses require the sample to be initially placed at the center of the target head; otherwise, the ion beam spot will trace out an arc on the sample surface during alignment procedures. This will result in continuous sampling of various target volumes rather than the single-volume element desired. Typical ion beam areas on target are approximately 1.5 mm^2. Thus, many individual locations on a sample can be examined during a single analysis. Implants can be performed using a disposable target mask and shield over exposed areas of the target assembly head. This can permit sequential implants and analyses to be performed without disturbing the specimen. To limit unintentional beam heating, the power delivered to the target by the ion beam is limited to <1 W.

The second goniometer, displayed in Fig. 16, is a high-precision XYZ manipulator (Model HPT115), with a rotary motion attachment module, manufactured by Vacuum Generators Limited, Hastings. This instrument lacks the precision of the previously described goniometer but offers XYZ translation and an extended range of operating temperatures. Motion resolution for the X and Y stages is 0.005 mm, with a repeatability of 0.002 mm. A total translation along the Z-axis of 150 mm is possible, with a resolution of 0.005 mm and a repeatability of 0.010 mm. The basic manual XYZ movement module is attached to a 150-mm Conflat flange for connection to the vacuum system. Six 34-mm accessory ports ring the primary flange for service or sensing-device entry. The XYZ module terminates in a 70-mm Conflat flange suitable for the attachment of a high-precision rotary drive. A dual-axis rotary-drive module attached to this port permits a manual 0 to 360° primary rotation about the Z-axis and secondary manual motion about the orthogonal axis.

Two specimen attachment modules are available for use. The first, shown in Fig. 17, has the sample attachment plate on axis, permits 0 to

YP5061

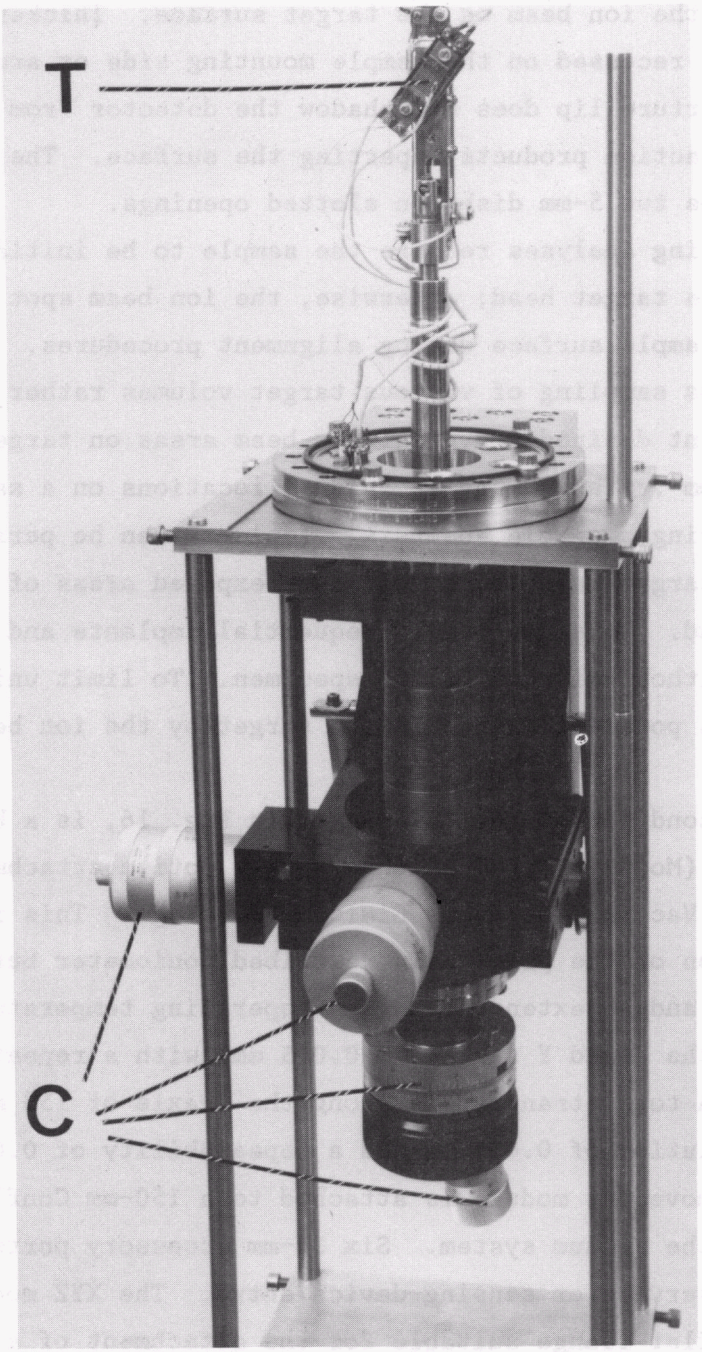

Fig. 16. Front view of the electron beam heated target assembly (T) mounted on the high-temperature translator. The x-y (top) and rotational (bottom) controls are shown by C.

YP5062

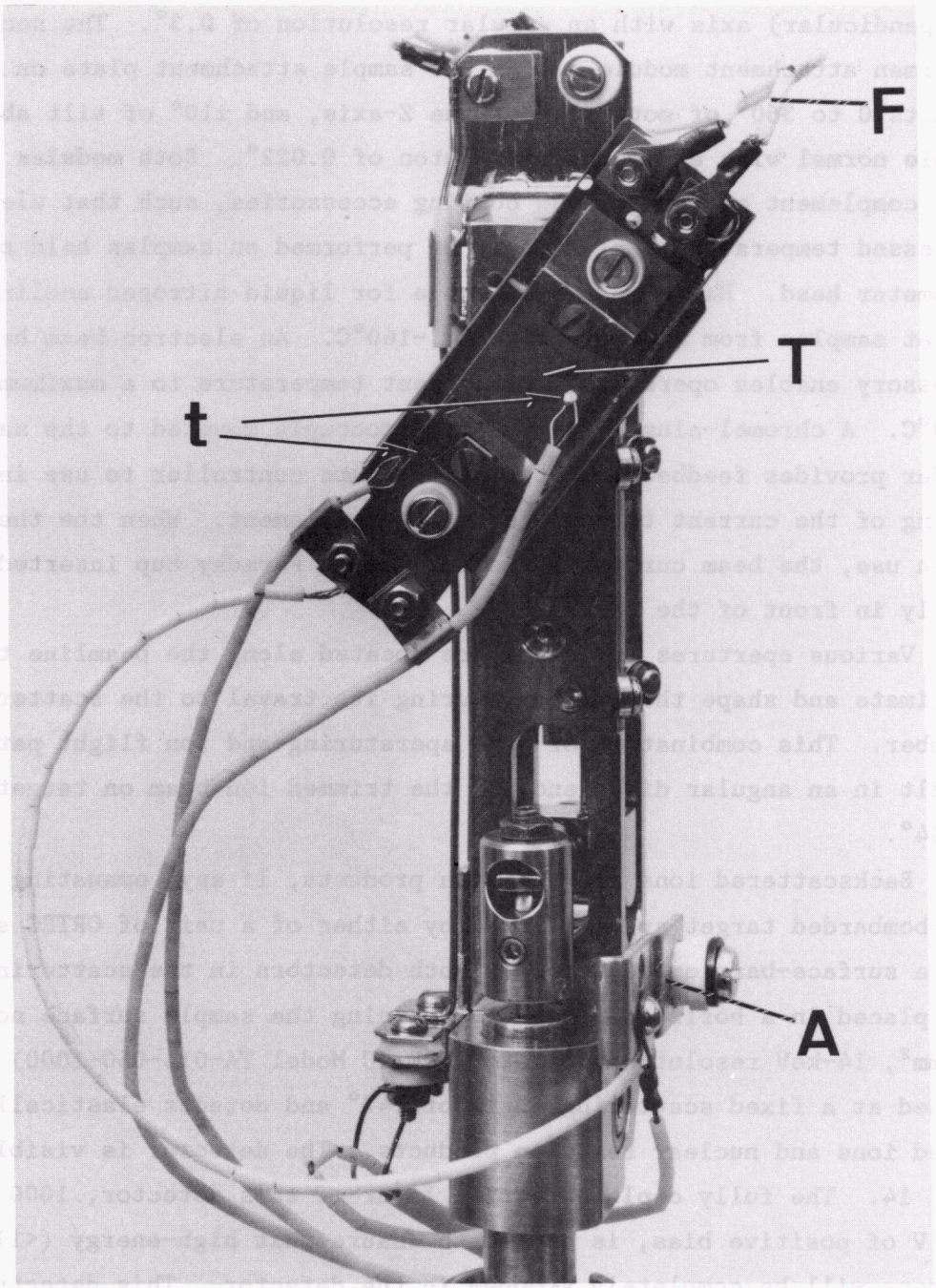

Fig. 17. Close-up view of the electron beam heated target assembly; F = filament leads, T = target area, t = thermocouple, and A = anode lead post.

360° of motion about the Z-axis, and ±90° of motion about the azimuthal (perpendicular) axis with an angular resolution of 0.3°. The second specimen attachment module places the sample attachment plate on axis, permits 0 to 360° of motion about the Z-axis, and ±10° of tilt about the sample normal with an angular resoluton of 0.022°. Both modules accept a full complement of heating and cooling accessories, such that elevated or depressed temperature implants can be performed on samples held on the gomometer head. Hardware is available for liquid nitrogen cooling of target samples from ambient to below -160°C. An electron beam heating accessory enables operation from ambient temperature to a maximum of 1200°C. A chromel-alumel (type K) thermocouple mounted to the sample holder provides feedback for the temperature controller to use in regulating of the current to the electron gun filament. When the thermocouple is in use, the beam current is measured by a Faraday cup inserted momentarily in front of the target.

Various apertures and slits are located along the beamline to collimate and shape the ion beam during its travel to the scattering chamber. This combination of slit aperaturing and ion flight paths can result in an angular divergence of the trimmed ion beam on target of <0.04°.

Backscattered ions and reaction products, if any, emanating from the ion-bombarded target are collected by either of a pair of ORTEC solid state surface-barrier detectors. Both detectors in the scattering chamber are placed in a horizontal plane containing the sample surface normal. A 50-mm^2, 14-keV resolution detector (ORTEC Model TA-014-050-1000) is positioned at a fixed scattering angle of 147° and detects elastically scattered ions and nuclear reaction products. The detector is visible in Fig. 14. The fully depleted active layer of this detector, 1000 μm for 300 V of positive bias, is chosen to ensure that high-energy (<11 MeV) protons will be completely stopped in the detector. This detector is apertured to 5.16 by 2.03 mm (10.5 mm^2) with a thick tantalum mask and presents a solid angle of 4.19 msr to scattered ions. The acceptance angle of the masked detector contributes to kinematic broadening in the scattered energy spectrum and is 2.36° for this detector. This back-angle detector can be masked from the backscattered beam by a thick tantalum shield situated on a linear motion drive. This permits implants to be

performed with heavy gaseous ions while effectively isolating the back-angle detector from elastic scattering events. A second 50-mm^2, 13-keV resolution surface-barrier detector (ORTEC Model TE-013-050-300) is located at a fixed-forward scattering angle of 56°. Full depletion of a 300 μm active layer requires 130 V of positive bias. The mask aperture is covered by a 6-μm-thick aluminized mylar window to prevent elastically scattered projectiles from entering and saturating the detector and detection electronics with high count rates. See Appendix E for procedures used to take scattering and channeling spectra.

3.4. FUTURE TRIPLE ION BEAM CHAMBER DESIGN

The existing triple-beam chamber is a modification of the dual-beam chamber in ref. 9. This chamber has limited flexibility and is inefficient; further modification would be impractical. A new chamber is needed to incorporate advances in surface modification technology such as ion-beam treatments of thin films. A new chamber will allow specimens to be processed more efficiently in a variety of ways and under improved vacuum conditions.

The new chamber is shown in Fig. 18. It consists of three principal modules: an entry/evaporation chamber, a bombardment chamber, and an Auger spectroscopy chamber. Rapid access to the first module is offered by the right-most gate valve in Fig. 18; pumpdown from air is carried out by the attached turbopump/mechanical pump combination (Balzers TPU 510 turbopump with 500 ls^{-1} capacity backed by a Model DUO 16B pump). Besides serving as an airlock entry to the adjacent modules, this chamber will be equipped with a small electron beam furnace for the in situ evaporation of films.

The center module, pumped by an Air Products AP-8 1000-ls^{-1} cryopump, is the main bombardment chamber with ports for the three beamlines and observation by infrared pyrometer, thermocouple, and other signal leads.

Further to the left side of Fig. 18, and again isolated by a gate valve, is the Auger/sputtering chamber that requires the ultrahigh vacuum pumping of a Varian 400 ls^{-1} Model 912-7022 VacIon pump plus a titanium pump, both mounted on the cross on the far left. The new differentially

YP4197

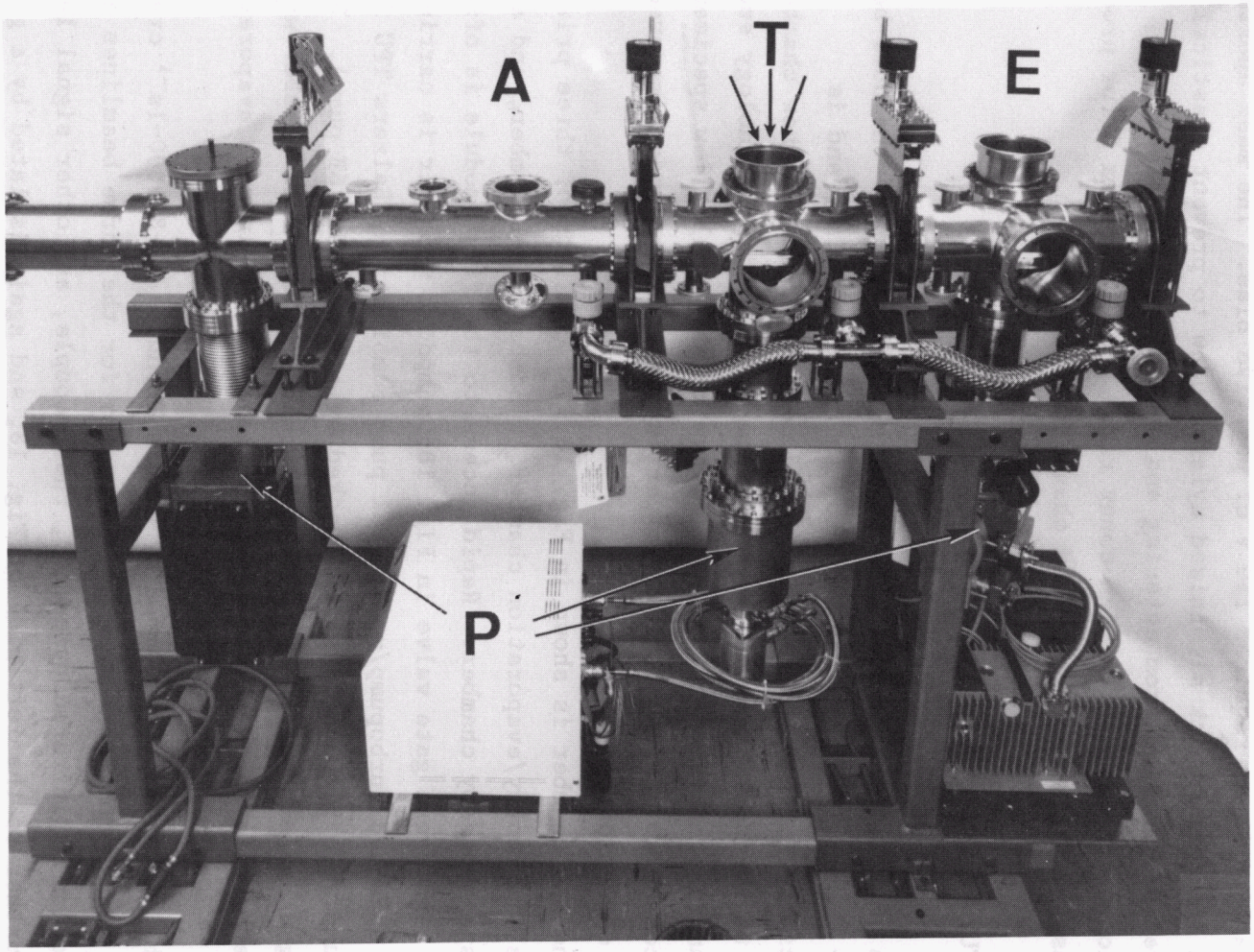

Fig. 18. Newly designed triple ion beam chamber consisting of the entry and evaporation chamber (E), the three-beam target chamber (T) and the Auger chamber (A). The three pumping stations (P) are shown as ion (left), cyro (center), and turbo (right).

pumped sputter gun (Perkin Elmer Model 04-300) is intended mainly to permit the depth-profile Auger electron spectroscopy (AES) study of specimens treated in the previous chambers (with no intervening air exposure).

Common to all three modules is a specimen transport system based on rigid, cruciform-section track segments and a worm-gear-driven trolley. The trolley "car" will mount five adjacent specimen positions, each presenting a 1-cm^2 specimen area for single, dual, or triple ion irradiation. Behind the central position in the bombardment chamber will be an electron beam specimen heater similar to the present heaters in Fig. 10, permitting bombardment temperatures from 400 to 800°C.

Final work on the specimen heating and instrumentation systems is in progress. When the chamber becomes operational, it will normally be situated with the three ion beamlines entering the central module. However, the entire assembly is mounted on a frame with "airfloat" pads beneath the feet, so that lateral translation can permit the beamlines to be attached to the first module instead. In that arrangement, simultaneous film evaporation and ion beam implantation/mixing processes can be carried out.

3.5. AUGER ELECTRON APPARATUS

Auger electron spectroscopy (AES) is a surface-sensitive analytical tool planned for in situ examination of near-surface regions modified by ion beams in the triple-beam chamber discussed in the previous section. AES is a true "surface" technique that provides improved depth resolution and greater sensitivity to light elements in a higher mass host matrix. The latter is a major shortcoming of Rutherford backscattering, since the elemental detection limits are a sensitive function of the atomic numbers of target components.

The critical component of a typical AES system is a cylindrical mirror analyzer (CMA) such as that manufactured by the Physical Electronics Division of Perkin-Elmer Corporation. The CMA consists of focusing optics to energy analyze the emitted Auger electrons and also houses an electron gun to provide a primary electron beam for excitation of Auger processes. The internal electron gun is mounted with its optical axis coincident with

the CMA symmetry axis. The beam of the internal electron gun is focused to a micron-size point on the surface of the specimen at the source point of the CMA. The energy analyzer of the CMA consists of a pair of coaxial metal cylinders. The outer cylinder is negatively biased, the inner grounded, and the electric field between the two determines the specific energy range of electrons selected by the CMA. Auger electrons ejected from the sample surface pass through an entrance aperture on the inner cylinder of the CMA. These are energy separated and directed through an exit aperture on the inner cylinder to an electron multiplier. The band of energies transmitted is related to the instrument resolution. The Auger electron signal is commonly recorded by electronically differentiating the number of Auger electrons as a function of the transmitted electron kinetic energy. The analog differentiation is performed by applying a small ac voltage on the outer cylinder of the CMA and synchronously detecting the output of the electron multiplier with a lock-in amplifier. The number of secondary electrons from the electron multiplier is recorded as a function of the Auger electron kinetic energy. Depth analysis is performed by cyclically monitoring the peak-to-peak Auger signal in selected energy windows as the sampled area is eroded by thousand-electron-volt ion sputtering. Stringent vacuum requirements for AES in the 10^{-10} torr range lessen the effects of contamination by an adsorbed species on a specimen surface. The combination of backfilling with inert argon and pumping active gases somewhat relaxes the vacuum requirements, since the concentration of surface gas impurities can be maintained at a lower level. Details of operating procedures for the Triple Ion Laboratory AES system are given in Appendix F.

A typical AES spectrum is displayed in Fig. 9. The spectrum is plotted as the differential number of Auger electrons, dN(E)/dE, as a function of Auger electron kinetic energy, E. A series of prominent peaks occur in the spectrum of Fig. 19. Electronic differentiation emphasizes these peaks by removing the large background consisting of elastically scattered primary electrons and inelastically scattered Auger electrons. The peak energies are characteristic of the energy levels of each atom type within the solid and are classified according to the three electron

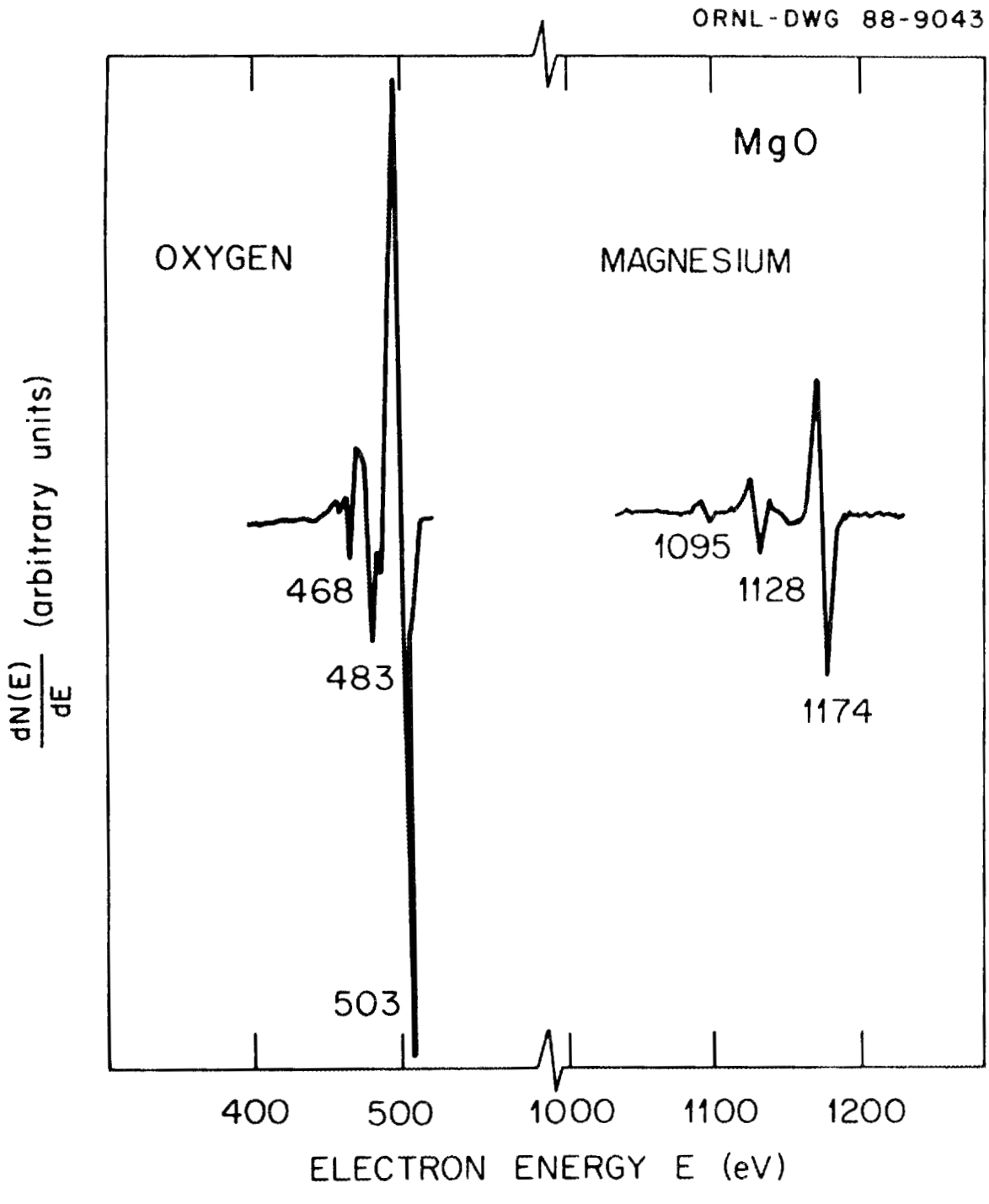

Fig. 19. Typical Auger analysis spectrum of a pure MgO single crystal. The primary lines in the spectrum are the 503-eV KLL oxygen line and the 1174-eV KLL magnesium line.

orbitals participating in the Auger electron ejection process. *The Handbook of Auger Electron Spectroscopy* (see Appendix F) is a reference book of standard data for identification and interpretation of AES data. Energies of the prominent Auger transitions for the components of the binary ceramic MgO are labeled in Fig. 19. There are three prominent Auger transitions of varying magnitude for oxygen near 500 eV and magnesium near 1150 eV. The Auger peak amplitude depends totally on the ionization cross section of the core-level electron. To monitor any variation of composition with depth, for this sample, energy windows would be set on the multiplexer to enclose the major oxygen and magnesium peaks. The peak-to-peak amplitudes would then be measured as the sample is eroded by sputtering.

4. RESEARCH APPLICATIONS WITH THE DUAL ION FACILITY

4.1. DUAL ION IRRADIATION EFFECTS ON VOID SWELLING

Prior to the recent upgrade and reconfiguration of the laboratory to a triple-beam facility, a large number of experiments were carried out for more than a decade using the dual-beam facility, consisting of the 5-MV and 400-kV machines. Generally, studies were aimed at exploring the fundamental mechanisms of helium and, to a lesser extent, hydrogen effects on radiation damage, and providing the experimental bases for theoretical correlations of void swelling and other effects with corresponding results for neutron irradiations.[10] An early study of this type is represented in Fig. 20.[11,12] That investigation revealed a marked dependence of the damage microstructure on the method of introducing gas. Such a result underscores the value of dual-ion bombardment capability, which allows full control over the gas introduction process.

4.2. TWO-COMPONENT BEAM METHOD

Since the masses of diatomic deuterium and that of atomic helium are equal, they can be accelerated together and steered onto the target. Immediately upon impact with the target surface, the molecular deuterium will dissociate into atomic species, each with half the beam energy. The

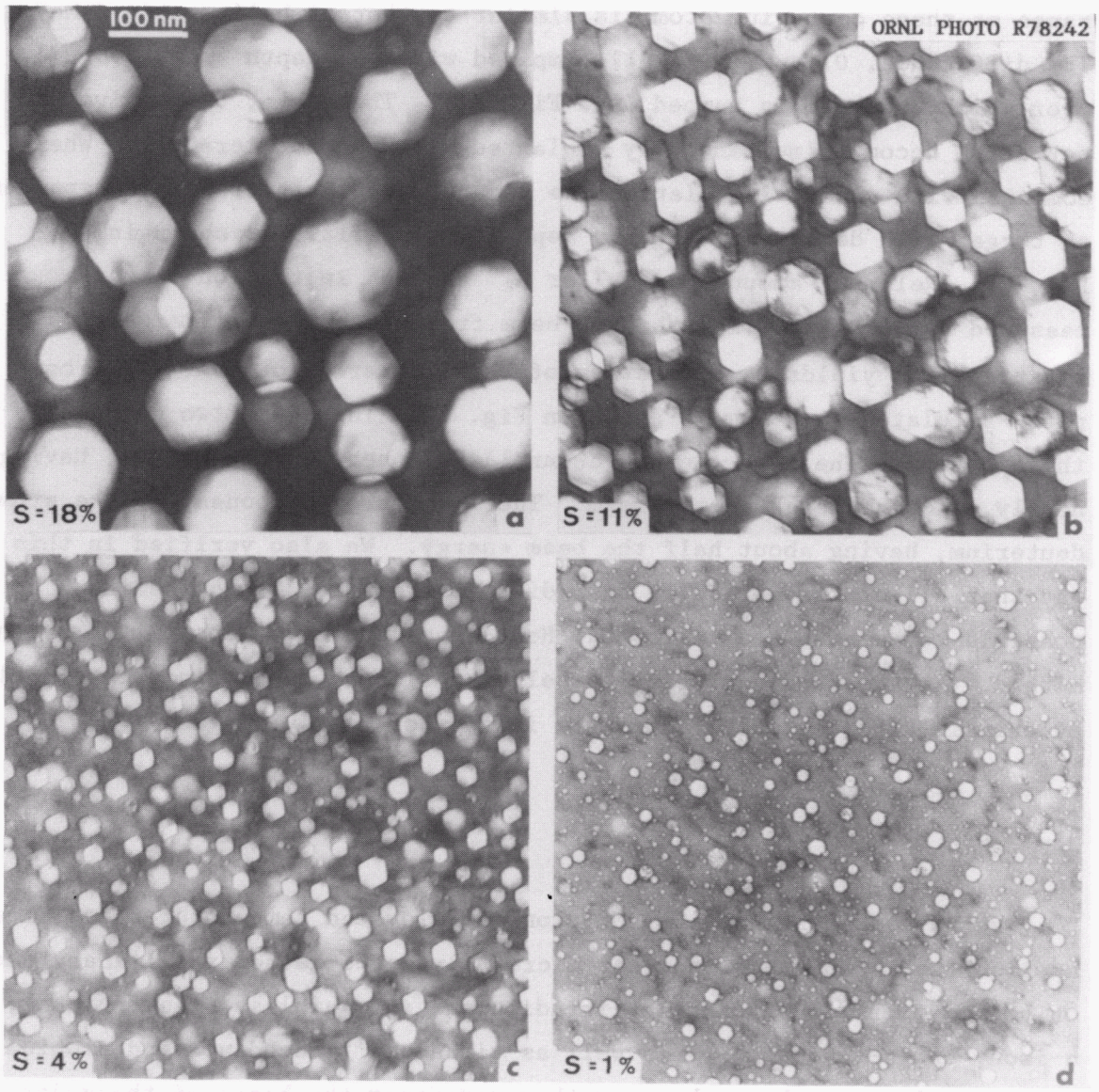

Fig. 20. Dependence of void swelling on the method of introducing gas in an austenitic alloy similar in composition to type 316 stainless steel. Without adding gas, case (a), bombardment with 4-MeV nickel ions to a damage level of 70 dpa at 900 K produced a swelling S of 18%. Simultaneous injection of helium at a rate of 20 appm/dpa of damage (a fusion reactor environment) gives rise to 11% swelling, case (b); whereas, simultaneous injection of 20 appm helium plus 50 appm deuterium per dpa (not shown) yielded 13% swelling. Preinjecting the same total amount of helium (1400 appm) resulted in much reduced swelling: in (c) hot pre-injection (900 K) resulted in 4% swelling; whereas, preinjection at room temperature (d) produced the most profuse cavity nucleation and a swelling of only 1%.

range of these deuterium atoms is similar to that of helium at 0.3 MeV. The difference, 0.1 μm, is small compared with the depth span (0.5 μm) over which the beam is ramped (see Fig. 21). Therefore, the helium and deuterium become simultaneously implanted with one accelerator.[2] When combined with nickel irradiation, we have three simultaneous atom species on target with density and energy deposition profiles as shown in Fig. 21. Relative amounts of D_2^+ or H_2^+ and He^+ in the ion beam are measured by backscattering the ion beam from a heavy-metal target and measuring the yields as a function of backscattered ion energy. A computer simulated spectrum is shown in Fig. 22. There are two components in the spectrum. The high-energy (channel) component is the helium, having nearly as much energy as the beam. The low-energy component is the atomic deuterium, having about half the beam energy. We also verified in this way that all of the molecular beam dissociated into atomic species. It is possible to measure the ratio $^4D_2$:^4He to an accuracy of about ±10% by this method. Any desired deuterium-to-helium ratio may be obtained empirically by changing the deuterium admixture in the helium source gas.

4.3. DIFFUSION OF HELIUM

We have used helium implantations at elevated temperatures and have applied the technique of nuclear microanalysis to gather preliminary data on helium migration during hot irradiations in stainless steel, nickel, α-iron, and α-zirconium,[13] as well as titanium,[14] vanadium, and niobium.[15] These metals were chosen because they represent the bases of the major alloys used in reactor structural components. They also display a wide range of responses to radiation damage. Stainless steels and nickel are highly susceptible to swelling and helium embrittlement, whereas ferritic steels are more resistant, and α-zirconium is comparatively immune unless considerable helium is introduced. One purpose of these experiments was to seek a correlation of helium migration with the known damage responses.

Targets were implanted with monoenergetic beams of helium-3 at energies of 200 or 300 keV. The helium was implanted at a flux of $\sim 3 \times 10^{16}$ helium ions ($m^2 s$) for a period of 1 h, which produced a calculated peak helium density of a few tenths atomic percent (depending upon the material) if no diffusion took place during the implantation.

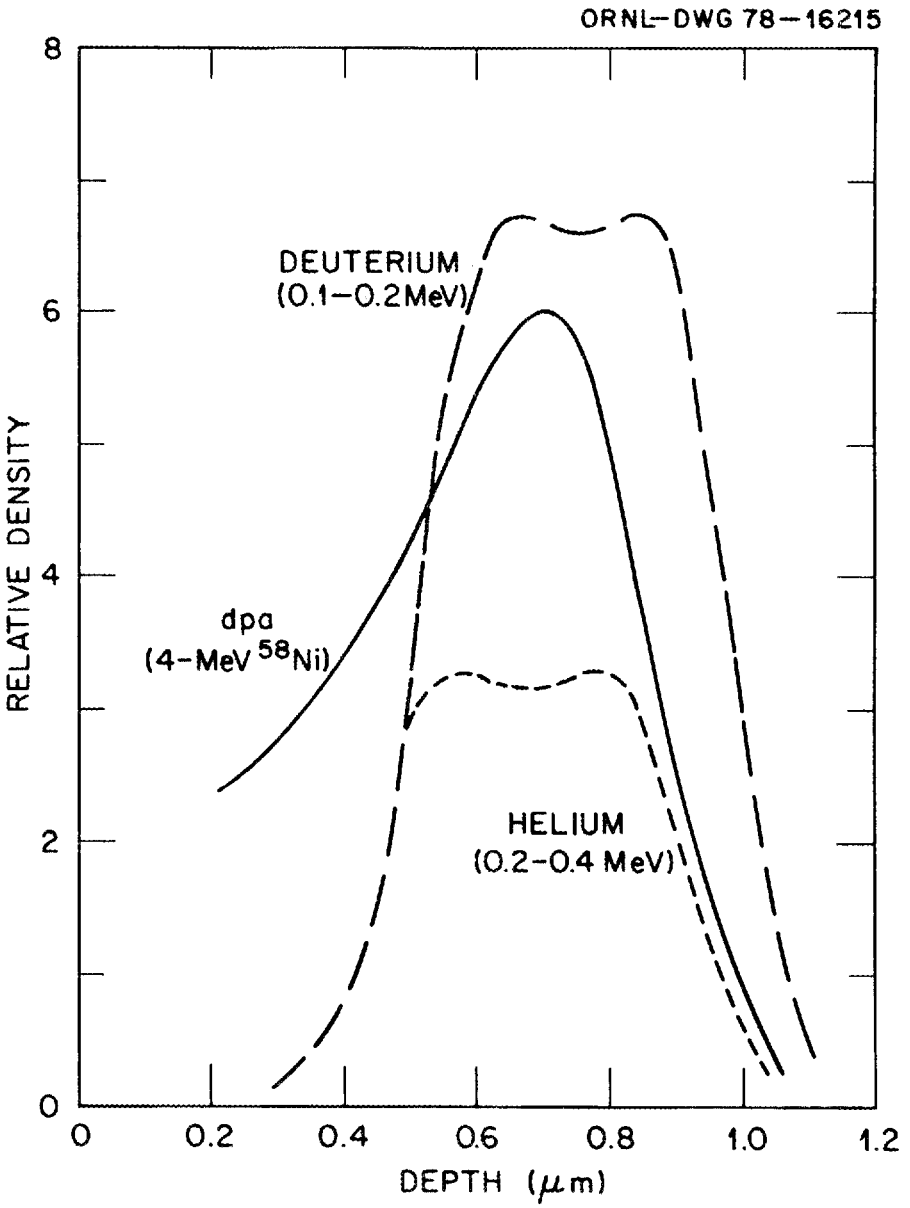

Fig. 21. Calculated profiles of helium and deuterium based on a simultaneous implantation of atomic helium and diatomic deuterium in which the accelerator energy is varied sinusoidally between 200 and 400 keV. The implanted profile spans the region of highest radiation damage (dpa) from 4-MeV nickel ions, as discussed in the text.

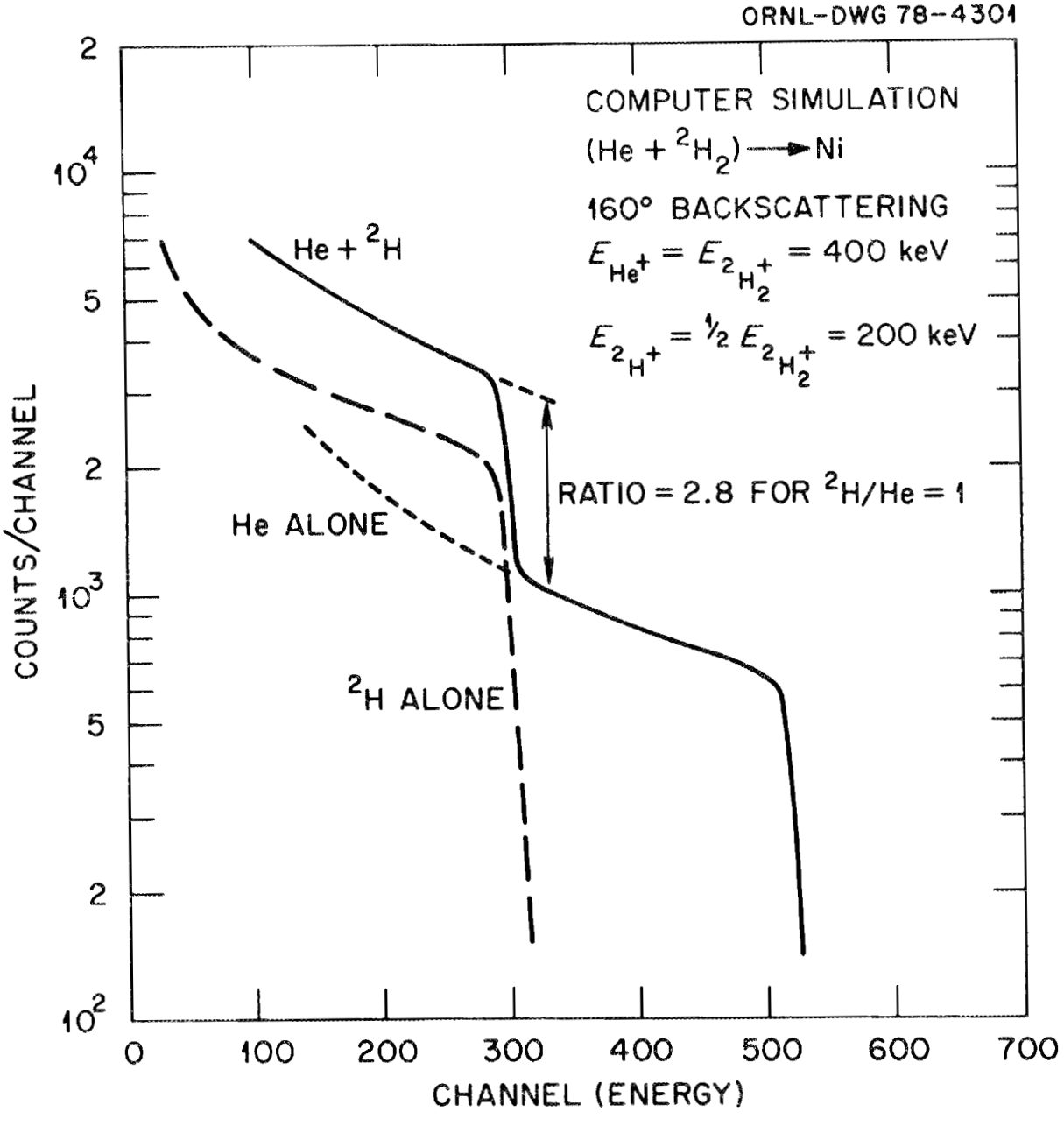

Fig. 22. Computer simulation of a typical backscattering spectrum from a beam of atomic helium and diatomic deuterium incident upon a nickel target.

Following the implantation, the targets were quickly brought to room temperature and transferred to a scattering chanber to determine concentration-depth profiles. In the scattering chamber (see Sect. 3.3), a 0.5-MeV deuterium beam was directed onto the target specimen. The $^{3}He(d,\alpha)$ reaction took place in the region where helium was concentrated. By measuring the energy of the alpha particles, the profile of the helium was determined.

These experiments chart the movement of helium under conditions of temperature and lattice displacement damage that are relevant to high-temperature reactor service. It is evident from the results shown in Fig. 23 that there are considerable differences in the temperature dependencies of helium migration in the various metals tested. In nickel and austenitic stainless steel, there is little migration of helium during irradiation up to the maxium test temperature of 973 K. In α-iron, significant migration begins between 773 and 898 K, and in α-zirconiun, the helium becomes mobile above about 700 K. Additionally, helium leaving the implanted regions is captured at the surfaces of the iron and zirconium targets. This is especially pronounced in zirconium.

4.4. DUAL-PULSED ION IRRADIATION EFFECTS ON PHASE STABILITY

Research using the dual-beam facility was among the first efforts to show that helium has extreme effects on phase stability during irradiation. Continuing research using this facility has provided the most systematic information on the effects of helium on phase stability. Some observed effects include suppression of radiation-induced precipitation, alterations in the sequence of phase transformations, and changes in the mixture of types as well as changes in the composition of phases.

An example is a nickel-ion bombardment experiment on a titanium-modified type 316 stainless steel, with and without simultaneous helium injection at a rate of 20 appm/dpa. Figure 24 shows some of the results.[16] On the left are the results for nickel ions only; on the right are those for the simultaneous irradiation. With no helium the precipitates are mainly G-phase, a true radiation-induced, nickel-rich silicide that contains about 50 at. % nickel and 30 at. % silicon, whereas the matrix contains only 15 at. % nickel and 2 at. % silicon. With helium, however,

88-17302

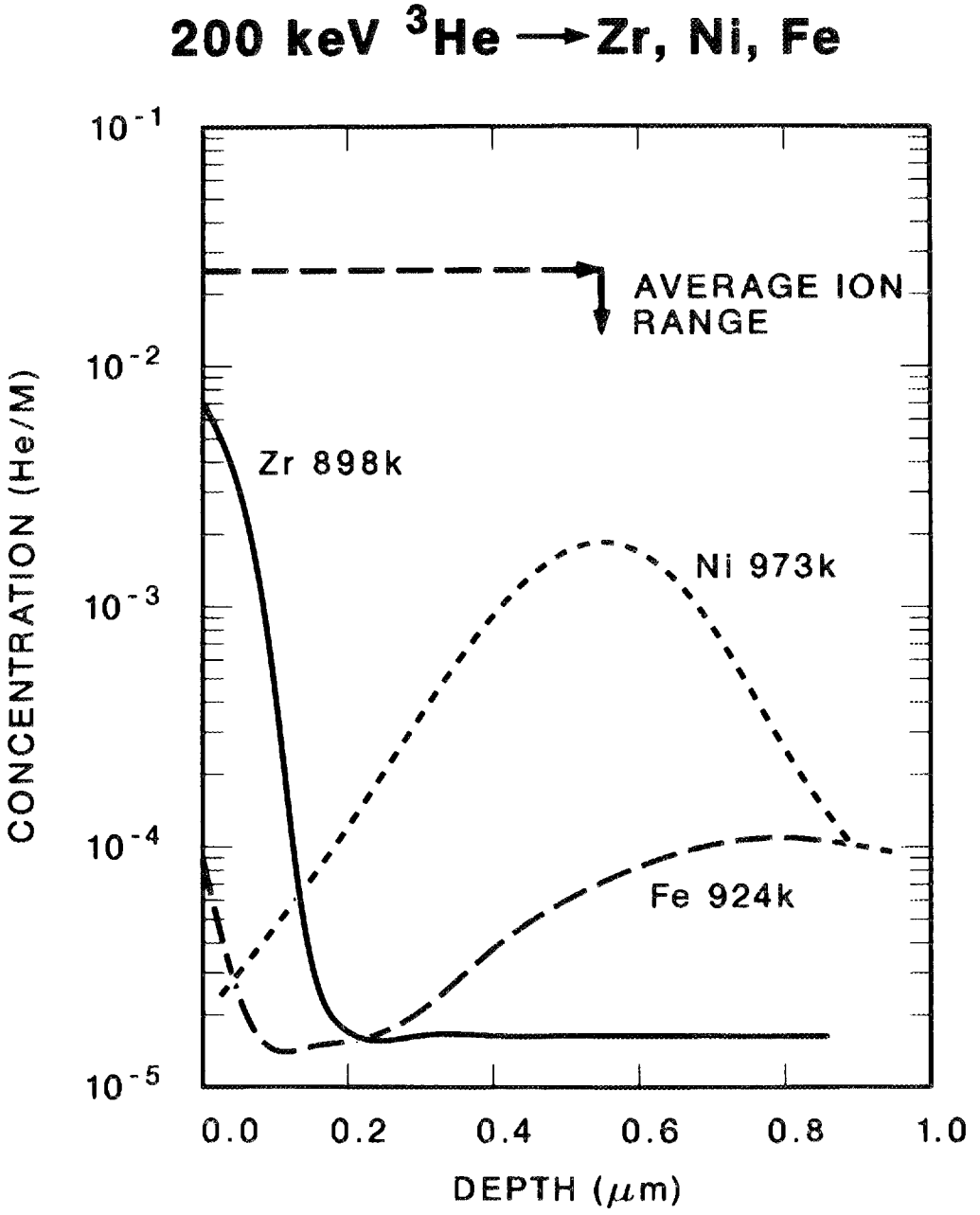

Fig. 23. Helium concentration-vs-depth profiles following high-temperature helium implantation into hcp zirconium, fcc nickel, and bcc iron.

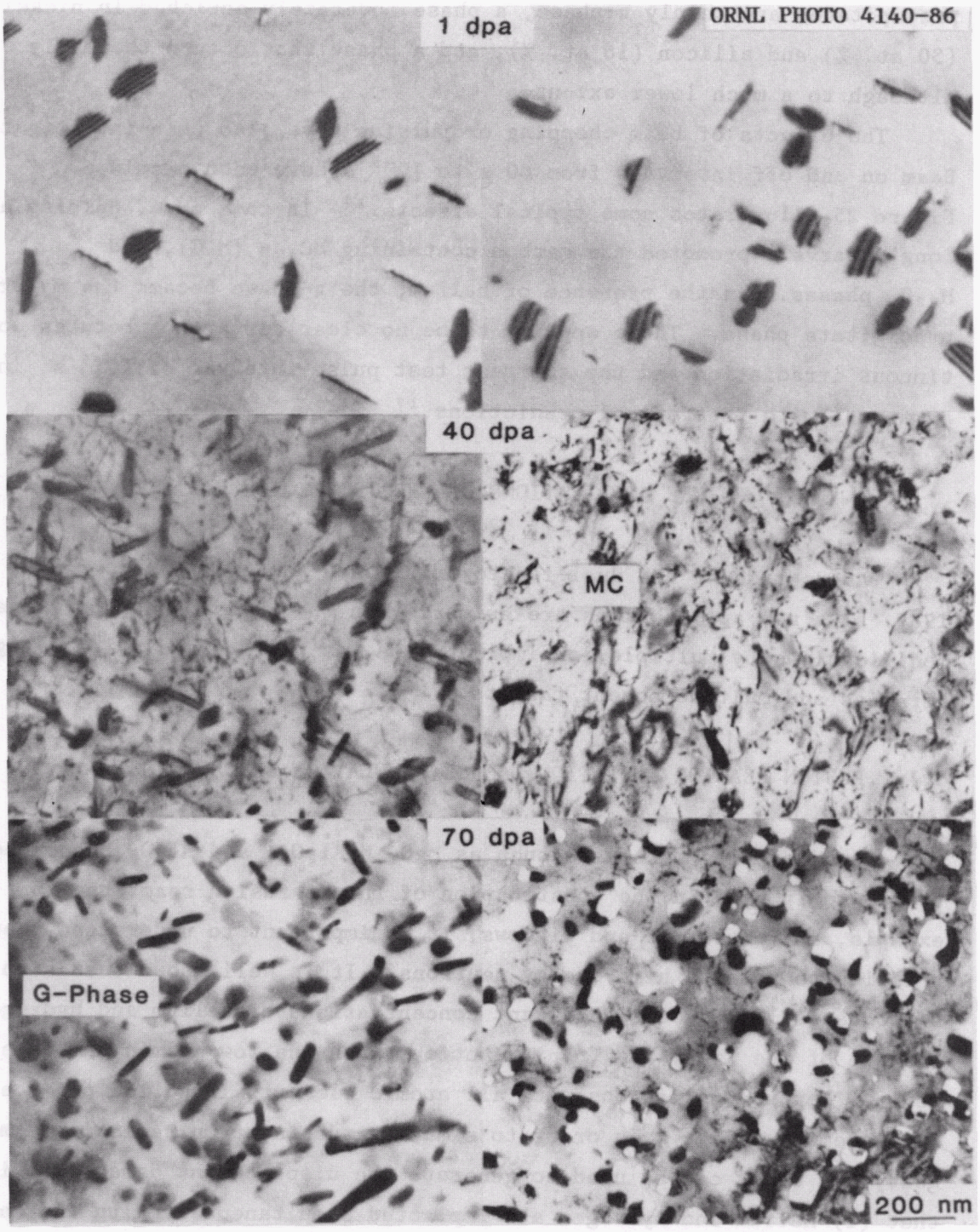

Fig. 24. Titanium-modified stainess steel irradiated to 1, 40, and 70 dpa at 675°C with 4-MeV nickel ions with simultaneous helium injection (right column) and without helium injection (left column).

precipitates are mainly η-phase, a phase moderately enriched in nickel (30 at. %) and silicon (16 at. %), and a phase that occurs thermally, although to a much lower extent.

The effects of beam chopping or pulsing have also been investigated. Beam on and off intervals from 60 s to 10^{-5} s have been examined. Figure 25 illustrates some typical effects.[17] In this case, pulsing at long intervals promoted the carbon containing MC, η (M_6C), and $M_{23}C_6$ phases. In the presence of helium, the η-phase became the major precipitate phase. There appears to be no clear difference between continuous irradiation and the shortest test pulse interval of 10^{-5} s, in agreement with theoretical predictions.[17]

5. FUTURE APPLICATIONS OF THE TRIPLE ION FACILITY

The upgrade of the dual-ion to triple ion facility was completed in 1987. Its new applications are primarily in the areas of compositional modifications by multiple-ion implantation, as well as radiation damage of ceramics and multicomponent targets.

5.1. FUSION REACTOR RADIATION DAMAGE SIMULATION IN CERAMICS

Since ceramic materials such as MgO, $MgAl_2O_4$, and Al_2O_3 are expected to be widely used in the construction of future fusion reactors, for example, as insulators and windows, it is important to understand their reaction to intense high-energy neutrons. It is well known that such neutrons will produce significant concentrations of helium and hydrogen because of the (n,α) and (n,p) reactions with the low-atomic-number elements. Neutron collisions with all atomic elements in solids produce displacement damage. In order to simulate such neutron radiation damage, heavy ion beams can be used to generate the displacement damage provided that (1) helium and hydrogen are implanted simultaneously with the heavy ions and that (2) the heavy ions once implanted do not significantly alter the stoichiometry of the ceramic target.

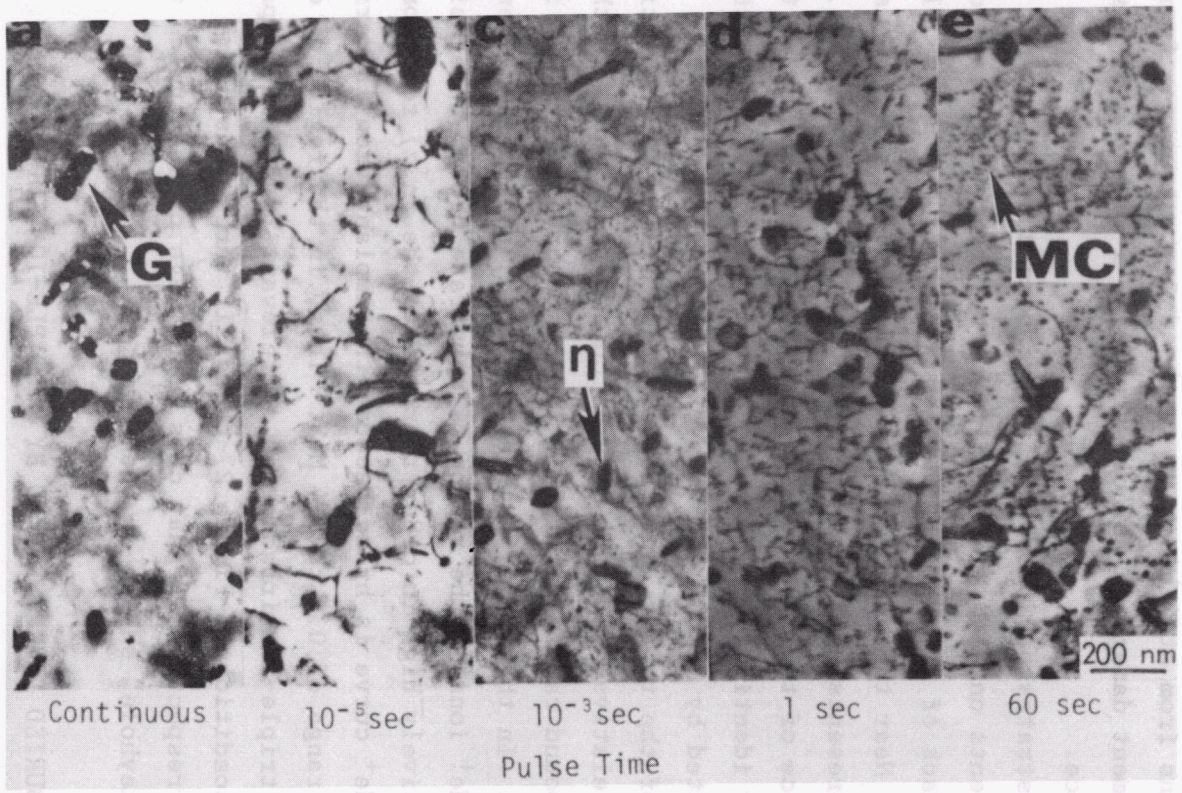

Fig. 25. Precipitates from 40-dpa bombardment with concurrent pulsed Ni^{2+} ions and He^{+} ions (to a final level of 800 appm helium).

The latter requirement can be fulfilled if the heavy-ion irradiation is carried out with both the cation-type (e.g., Al^+ or Mg^+) and the anion-type (e.g., O^+ or N^+) ion beams. The metal ion, gas ion, and helium-hydrogen ion beams can be tailored to satisfy requirements (1) and (2) above. In addition, the facility provides the capability to separate the effects of deviations from stoichiometry on the defect structure from the effects of displacement damage on defect structure, a question of basic scientific importance.

Figure 26 illustrates how these ideas have been used in recent triple-beam experiments on Al_2O_3. The solid curves represent displacement damage along the track of 2.0-MeV Al^+ ions and 1.4-MeV O^+ ions as calculated by EDEP-1.[18] Near the end of the range of these ions is a Gaussian-like curve that represents the depth profile of these deposited ions. Because of the choice of the relative ion energies, the profiles of the two ions are nearly identical. Due to the significant skewness of these profiles, as estimated by TRIM, some ions will be deposited in the shallower regions of the target, but the target stoichiometry can still be maintained if the relative beam intensity is chosen to be equal to the stoichiometric compound ratio for Al_2O_3. The last curve in Fig. 26 is the deposited He^+ ions. In this case, the energy of the helium is chosen purposely to deposit He^+ ions in the region of substrate depth where defect production is relatively high in order to simulate the (n,α) reaction noted above. The He^+ curve is broad because the implantation is carried out over an energy range of 0.2 to 0.4 MeV. Thus, in the region of depth 0.6 to 0.8 μm, the triple-ion irradiation is relevant to the anticipated reactor radiation conditions. Figure 27 shows all three ions beams illuminating their respective Faraday cups. An image of an alumina target can be seen as a "keyhole" shadow on the cups.

5.2. SURFACE AND BURIED LAYERS FORMED BY MULTIPLE-ION IMPLANTATION

In addition to producing highly defected surface regions, a primary use of ion implantation is to alter the chemical composition near the surface of the target material. In addition, this alteration can be carried out at both low and high target temperatures, and it can be done with small amounts of material over a narrow and controlled depth range; this

ORNL-DWG 88-8527

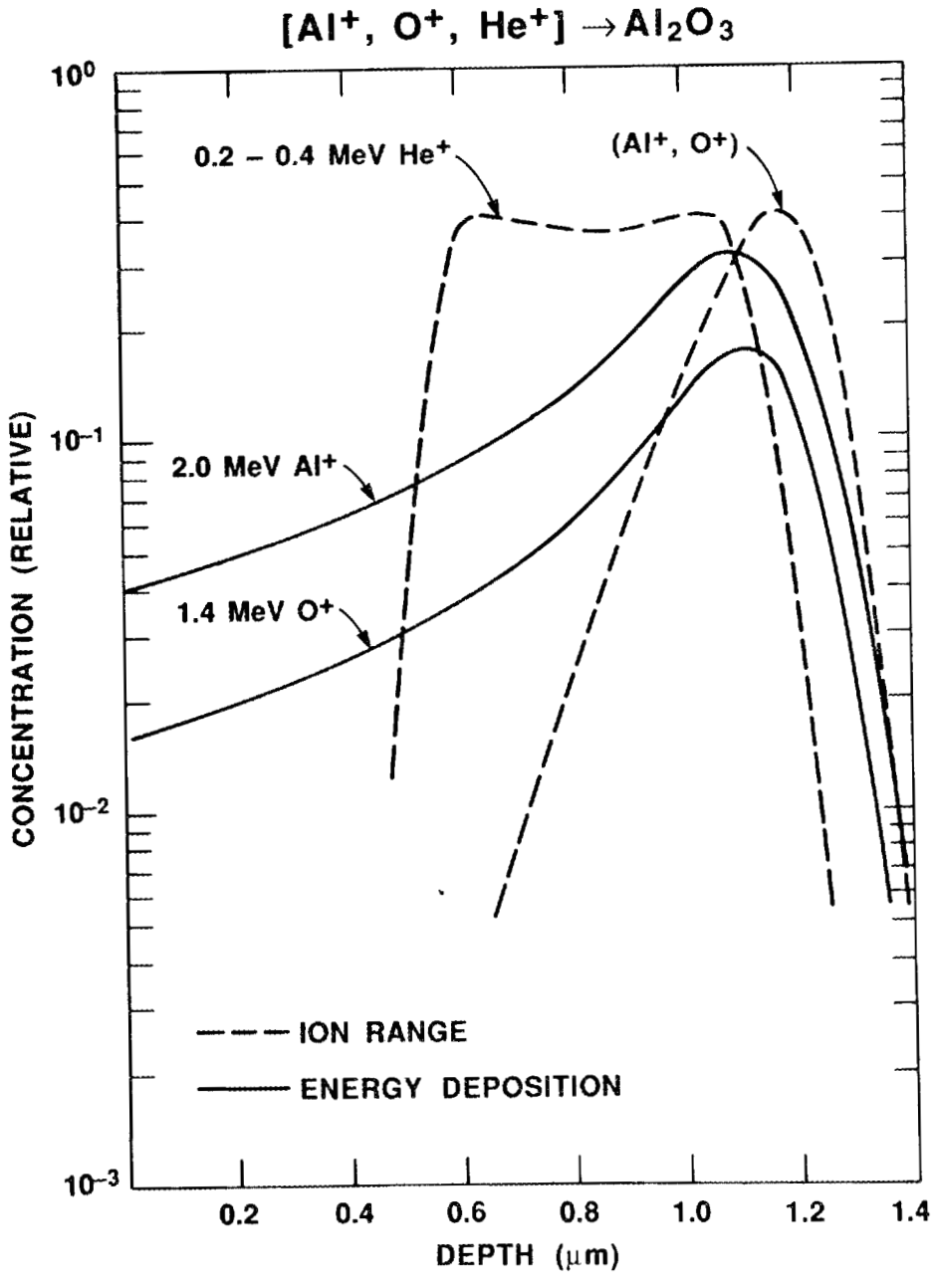

Fig. 26. Concentration-vs-depth profiles calculated for the case of triple-ion implantation of aluminum, oxygen, and helium into aluminum oxide crystal. The defect concentrations are given by the solid curves (helium is not significant). The implanted atom concentration profiles are given by the dashed curves. The helium curve is broad because the ions are not monoenergetic.

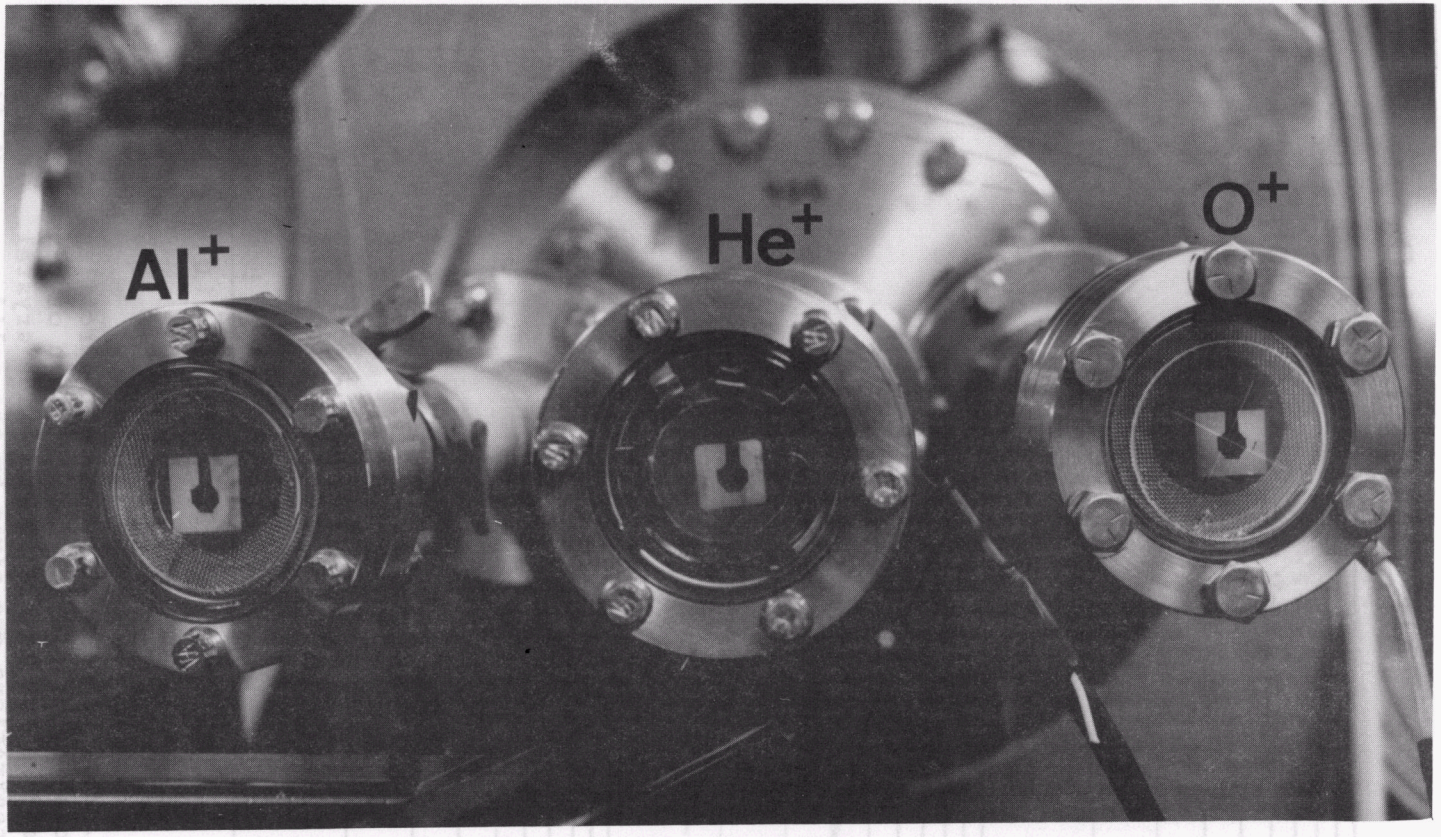

Fig. 27. Three ion beams of Al^+, O^+, and He^+ illuminating their respective Faraday cups, shown in Fig. 7. The target casts a "keyhole" shaped shadow on the quartz cups.

allows three-dimensional chemical alterations of the target. For example, a conducting buried layer can be implanted below the surface of a nonconducting target, or vice versa. Buried layers not only alter electrical properties but also mechanical properties such as tensile strength, fatigue, hardness, wear, and corrosion.

Some of the results of recent simultaneous dual-ion (B^+, N^+) implantations are given in Fig. 28. A ternary alloy (Fe-15Ni-13Cr) was implanted with 500-keV N^+ and 360-keV B^+ so that precipitate formation would be possible at the end of their ion ranges. As can be seen in Fig. 28, the hardness of the alloy is enhanced especially for the room-temperature experiment. When compared to single ion B^+ and N^+ implantation (not shown in Fig. 28), the dual-ion-implanted specimens also showed factor-of-2 increases in fatigue life; however, the single-ion-implanted specimens showed little change from the original virgin material (top of Fig. 28). Cross-sectional TEM of the dual-ion irradiated samples revealed extensive black dot features with no discernable precipitates. Optical microscopy and TEM of fatigued specimens showed numerous slip bands in both unimplanted and singly implanted specimens, in contrast with very few slip bands in the dual-ion implanted specimens. Numerous microcracks, in association with the slip bands, were observed after fatigue testing only in the specimens that were not implanted with dual ions, suggesting a mechanism of dislocation pinning by the dual-ion BN implantation. Simultaneous B, N, and C bombardments are now in progress.

6. REFERENCES

1. J. K. Hirvonen, ed., *Treatise on Materials Science and Technology, Vol. 18, Ion Implantation*, Academic Press, New York, 1980.

2. M. B. Lewis, N. H. Packan, G. F. Wells, and R. A. Buhl, *Nucl. Instrum. Methods* **167**, 233 (1979).

3. J. F. Ziegler, ed., *New Uses of Ion Accelerators*, Plenum Press, New York, 1975.

4. K. O. Nielsen, *Nucl. Instrum. Methods* **1**, 289 (1957).

5. C. D. Moak, H. E. Banta, J. N. Thurston, J. W. Johnson, and R. F. King, *Rev. Sci. Instrum.* **30**, 694 (1959).

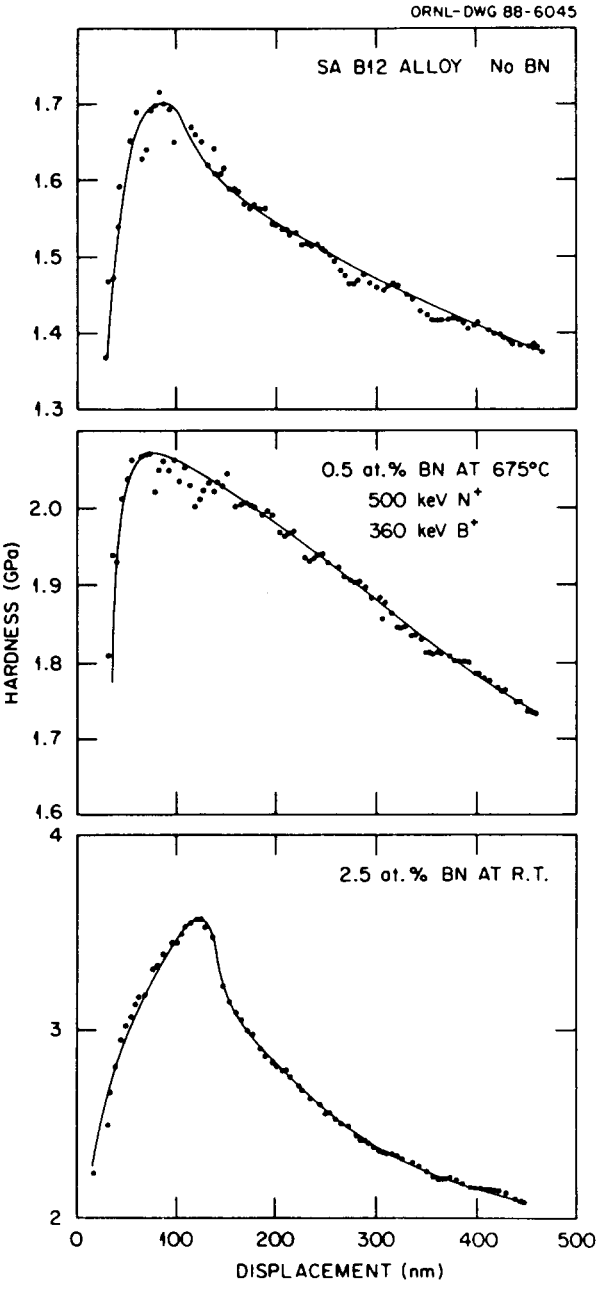

Fig. 28. Hardness measurements on the indicated alloy before and after simultaneous B^+ and N^+ ion implantation at 675°C (center) and at room temperature (bottom).

6. C. H. Johnson, *Nucl. Instrum. Methods* **127**, 163 (1975).

7. M. B. Lewis and G. K. Schulze, *Nucl. Instrum. Methods* **B9**, 100 (1985).

8. H. Oona and W. S. Bickel, *Rev. Sci. Instrum.* **47**, 517 (1976).

9. N. H. Packan and R. A. Buhl, *A Multispecimen Dual-Beam Irradiation Damage Chamber*, ORNL/TM-7276, June 1980.

10. L. K. Mansur, E. H. Lee, P. J. Maziasz, and A. F. Rowcliffe, *J. Nucl. Mater.* **141–143**, 633 (1986).

11. N. H. Packan, K. Farrell, and J. O. Stiegler, *J. Nucl. Mater.* **78**, 143 (1978).

12. N. H. Packan and K. Farrell, *J. Nucl. Mater.* **85–86**, 677 (1979).

13. M. B. Lewis and K. Farrell, *Nucl. Instrum. Methods* **B16**, 163 (1986).

14. M. B. Lewis, *Nucl. Instrum. Methods* **B22**, 499 (1987).

15. M. B. Lewis, *J. Nucl. Mater.* **152**, 114 (1988).

16. E. H. Lee, N. H. Packan, and L. K. Mansur, J. Nucl. Mater. **117**, 123 (1983).

17. E. H. Lee, N. H. Packan, M. B. Lewis, and L. K. Mansur, *Nucl. Instrum. Methods* **B16**, 251 (1986).

18. I. Manning and G. P. Mueller, *Comput. Phys. Commun.* **1**, 85 (1974).

APPENDIX A

HEAVY-ION SOURCE OPERATION

A.1. MODEL 910 DANFYSIK SOURCE PREPARATION

The ion source shown in Fig. A.1 operates on the principle of an oscillating electron ionizer. Following is the procedure for assembling this source for use on the 5-MV accelerator. The surface of a new tungsten filament is chemically cleaned with a solution of boiling 20% KOH solution for 5 min. The filament is then placed in the source with the short post attached to the ground electrode and the long post to the positive voltage electrode. The filament is enclosed and centered in the graphite anode, which is the ion-chamber enclosure. Source material can be one or a combination of five forms: gas, powder, shavings, solid rod, or grid wire. The material used most often in the form of powder or shavings which is loaded into a quartz tube attached to a molybdenum gas inlet tube by a graphite holder. The top end is plugged with quartz wool to prevent chloride vapor from backstreaming, whereas a smaller plug of wool is placed at the bottom end to prevent the metal powder from entering the anode chamber. With rod-shaped source material, the rod is introduced into the ion chamber through an opening in the graphite anode wall. A wire grid is used to hold a foil of the material to be accelerated.[1] The grid is placed along the inner-wall surface of the anode (Fig. A.2).

There are two molybdenum inlet tubes that can feed gas directly into the ion chamber. When the source material is in the form of powder or shavings, the gas (usually CCl_4) is fed through the tube holding the source material in the quartz. With the dual molybdenum inlet tube arrangement, we have the capability of introducing different gas types at the same time. After the filament and source material have been properly placed and adjusted in the ion chamber, the assembly is moved into the source magnet housing. The housing is then placed on the accelerator tube stack, and the electrical and gas feed lines are attached. The source coolant lines are also attached at this time. The source is now ready to be evacuated and conditioned.

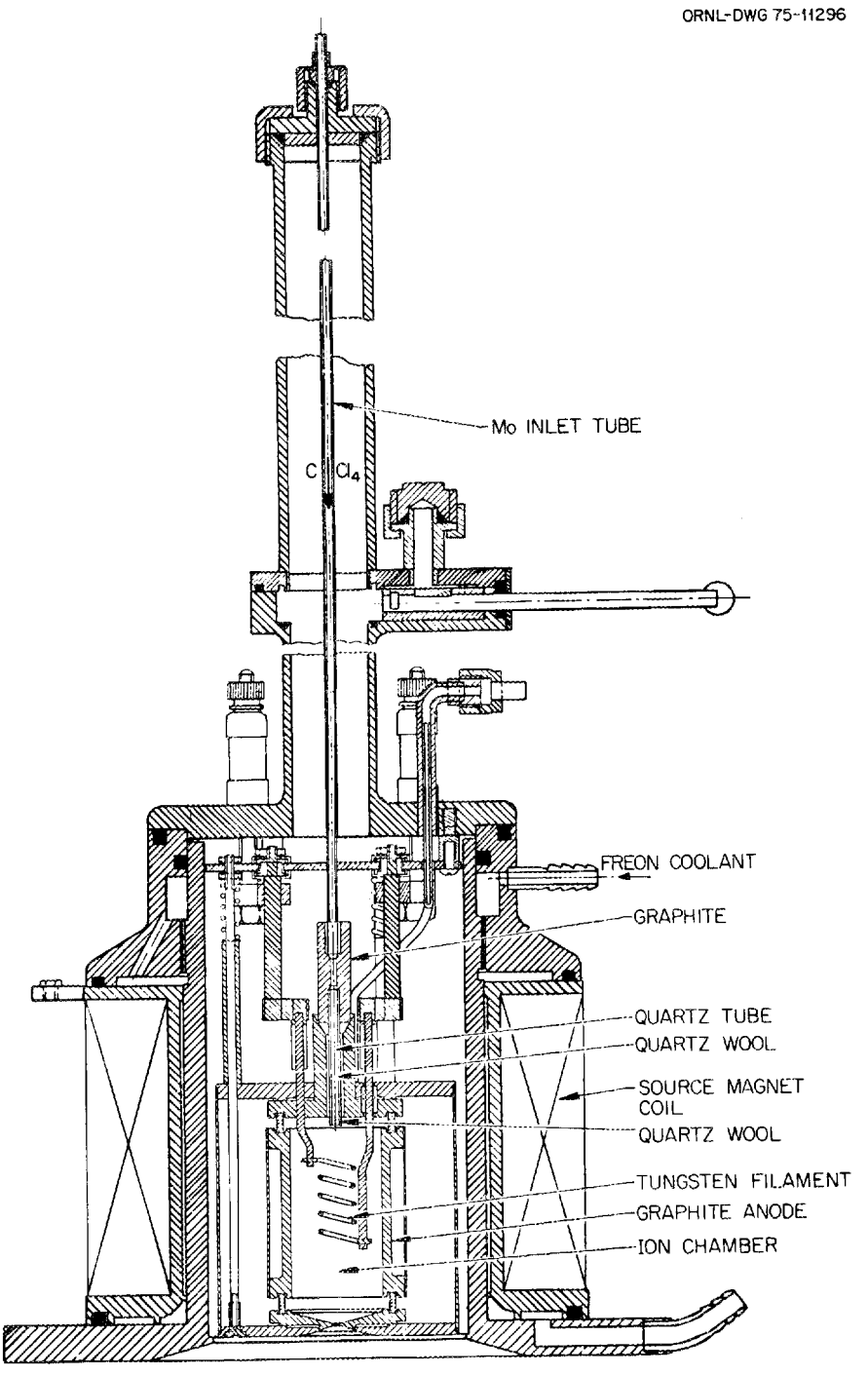

Fig. A.1. Basic component of the Model 910 Danfysik heavy-ion source.

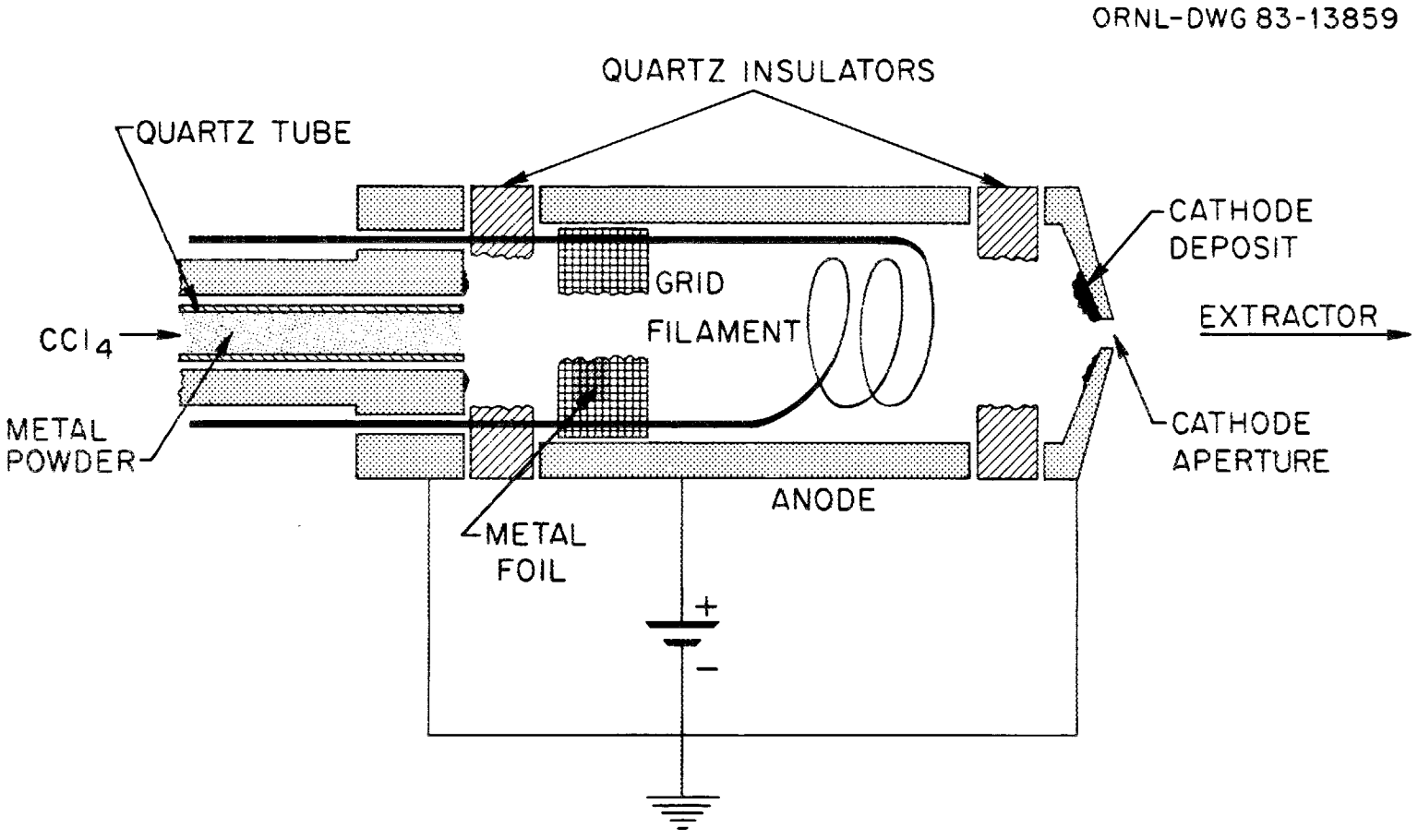

Fig. A.2. Detailed drawing of the graphite anode assembly shown in Fig. A.1. In this arrangement, a metal foil is held in place by a tungsten grid so that the foil is directly exposed to the source plasma.

A.2. PRINCIPLES OF HEAVY ION SOURCE OPERATION

A.2.1. Ion Extraction

During typical operation, the metal powder (M) and CCl_4 gas react to form $M + CCl_4 \rightarrow MCl_2 + Cl_2$. The MCl_2 vapor is then dissociated and ionized.

When, for example, the metal is nickel, the ^{58}Ni consumption for producing the ion beam is ≈2/3 mg/h. Another ≈2/3 mg/h of ^{58}Ni is consumed in $NiCl_2$ production, which backstreams and condenses in the quartz tube within the graphite coupler between the molybdenum inlet tube and the quartz tube. With an initial charge of, say, 200 mg of ^{58}Ni in the ion source, the average useful lifetime is about 80 h when operating with a normal beam of 1 particle microampere on target; lifetimes have ranged between 60 and 113 h.

The $NiCl_2$ formed in the source tube is dissociated and ionized by the action of an energetic electron current in the ionization chamber, shown in Figs. A.1 and A.2. A tungsten filament (1 mm in diameter) carries a typical load of 40 to 50 A at 8 to 10 V dc, causing the chamber temperature to rise to ~500°C. The electron emission from the filament is directed into an expanding spiral path by the action of the electric and magnetic fields in the chamber. The electric field vector is radial with respect to the beam axis, and its strength in the 2.7-cm-diam chamber is controlled externally by anode voltage. Since the first ionization potential of nickel is 5.4 eV lower than that of chlorine, the anode voltage is usually kept low, ~40 V. The magnetic field vector is axial with the beam, and its strength is determined by the currents in both the coiled filament and a solenoid mounted externally to the vacuum system, as shown in Fig. A.1. A typical solenoid current of 1.0 A produces a field of ~50 G in the chamber. The high filament current vectorially adds to the magnetic field in the centermost region of the chamber.

The spiraling motion of the electrons increases their path length and thereby increases the collision probability for ion production with high ionization efficiency. Under typical operating conditions, the electron density is high enough to produce a stable plasma whose ions will drift toward terminal ground at the chamber exit. The ions exit through a

1.5-mm diam hole at the base of the chamber and on the beam axis. This mechanism defines a sharp optical point and limits the kinetic and directional components of the emerging ions to very narrow spreads of <5 eV. The vacuum in the ion source region external to the anode chamber is $\sim 3 \times 10^{-5}$ torr under typical operating conditions.

The positively charged ions in the aperture region of the anode are extracted by a strong electric field set up by a conically shaped copper extractor. The extractor is 4 cm at the base and 1.2 cm at the top, with a 1.0-cm aperture through the 1.5-cm conical axis. The extractor carries a typical voltage of -20 keV relative to the anode, thus creating an electric field of 14 keV/cm in the 1.4-cm accelerating gap. In the centermost region of the field, a space charge equilibrium is established between positive ions issuing from the anode and backstreaming secondary electrons caused by some positive ions bombarding the surface of the extractor. The extractor has been modified from the original design. The present copper extractor is mounted on a thin-walled stainless steel tube in order to minimize thermal conductivity. In this way, the extractor surface maintains a high operating temperature ($\approx 500^{\circ}C$) because of its proximity to the hot anode and the absorption of some of the ion current. This condition eliminates the condensation of most metal chlorides on the extractor surface. A thin grayish film, believed to be mostly carbon, forms on the extractor surface; however, its formation does not seem to lower the extraction efficiency.

A.2.2. Ion Separation and Focus

The ionization and extraction system yields comparable fluxes of nickel and chlorine ions that must be separated prior to acceleration in order to avoid excessive accelerator tube loading. Also, the extraction process necessarily induces a high divergence in the beam. Controlling the divergence and focusing the beam are accomplished by the action of a three-cylinder einzel lens. The focal length of the lens is long enough ($\approx$20 cm) for an ion separator to be installed between the extractor and the gap lens, which is located just before the first stage of acceleration, as shown in Fig. 4 (in text). The potential on the two outer barrels of

the einzel lens is the same as the extractor voltage, whereas the inner barrel (length 6 cm, diameter 10 cm) is nearly ground (or ion source) potential. In its present design, the einzel lens is strengthened by the presence of a molybdenum screen (placed in front of the first barrel) that acts to reduce the radial electric field lines directed away from the beam axis.

The ions are separated by an electric-magnetic field velocity selector in which the action of the electric field is exactly nulled by the action of a perpendicular magnetic field for a given ion velocity (or mass); or

$$v = E/B \ ,$$

where v is the ion velocity, and E and B the electric- and magnetic-field strengths, respectively. The electric field is generated across two parallel copper plates that are 18 cm long, 1 cm wide, spaced 2 cm apart, and are oriented along the beam axis. The field strength is typically 300 to 400 V cm^{-1}. Fringe fields are reduced by mounting wires between the edges of the respective plates and holding an intermediate potential between them. The cross-field magnet is of the wire-wound iron-core type carrying about 5 A. The results of the ion separation are discussed in Appendix E.

The einzel lens must focus the ion trajectories to a crossover (or waist) at the aperture of the gap lens. This aperture is 5 mm in diameter and is located about 40 cm downstream from the inner einzel barrel.[2] The length of the accelerating gap is 1.5 cm, followed by an exit aperture of 1.7 cm. The gap lens typically operates at 10 keV. This action, along with the accelerator tube (fixed by the Van de Graaff voltage), acts to focus the beam to a waist at a point beyond the accelerator; for our purposes this point would be the focal point of the 90° energy-analyzing magnet shown in Fig. 2 (in text). The accelerating tube consists of 135 potential planes, each carrying an incremental voltage of about 30 keV.

A.2.3. Ion Beam Transport

The nickel beam produced by the accelerator source is primarily in a singlet charge state. Because of the combination of high mass and high

energy of the Ni^+ ions, conventional analyzing magnets do not have sufficiently high field strength to deflect them through 90°. In the present system, we have installed an ion stripper near the entrance to the magnet. In this way, the percentage of charge state 2^+ in the beam is increased to about 25%. The Ni^{2+} beam can be conveniently analyzed and is of sufficient intensity (5–10 μA) to be used for most bombardment needs. The stripper, located as shown in Figs. 1 and 3 (in text), consists of a differentially pumped cylindrical tube 35 cm in length and 1.6 cm in diameter. Argon gas is fed into the tube to maintain a stripping tube pressure of ≈0.1 torr, whereas the outer stripper pumping maintains the exterior vacuum to about 6×10^{-5} torr. Apertures 1 cm in diameter are mounted just above and below the stripper tube. The apertures serve both to define the beam direction through the stripper tube and to better confine the stripper gas. Using apertures in this manner, the accelerator tube vacuum can be maintained below 4×10^{-6} torr.

The 90° double-focusing analyzing magnet transmits only those ions with

$$\frac{mE}{q^2} = \frac{B^2R^2}{2} \leq 62 \ (\text{amu.MeV.e}^{-2}) \ ,$$

where R = 73 cm is the effective radius of curvature of the ion path in the magnet. Thus, the magnet uniquely selects the charge state of the beam and defines its energy. The magnet also acts as a lens of short focal length. The magnet pole face ends are cut 26° so that the symmetric object and image distances are 2 R from the pole faces. The focal lengths measured from the exit pole face are 0.67 R vertically and 0.35 R horizontally. The object of the magnetic lens is formed by focusing the gap lens so that it forms a beam waist near the center of the stripper. The magnetic lens image is then formed near the control slits, 55 cm from the magnet exit. The beam waist at this point is <2 mm, but the divergence (≈0.001 radians at the magnet entrance) increases to ≈0.005 radians, as expected from Lagrange's law.[3] The machine energy is maintained by the control slit feedback system. This regulation maintains a machine energy of 4 MV with a spread of about 5 kV.

A.3. REFERENCES FOR APPENDIX A

1. M. B. Lewis, *Nucl. Instrum. Methods* **219**, 247 (1984).

2. C. H. Johnson, J. P. Judish, and C. W. Snyder, *Rev. Sci. Instrum.* **28**, 942 (1957).

3. That is, the fundamental limitation relating the magnification or beam size and the divergence of the beam. For small divergence and in the absence of aberrations, $D\theta\ V^{1/2}$ = constant, where D, θ, and V are the beam diameter, divergence, and space potential. (See ref. 2 for further discussions and references.)

APPENDIX B

SOURCE CHANGEOVER PROCEDURE: FROM THE DANFYSIK TO THE DUOPLASMATRON SOURCE

To remove the source, the filament and anode electrical links must be disconnected, and the freon coolant lines must be detached. Electrical leads to the source magnet must also be disconnected, as well as the gas feed lines to the source. After the Danfysik source and magnet assembly have been removed from the tube stack, the Duoplasmatron source can be put in place. Before placing the Duoplasmatron source onto the tube stack, the Danfysik extractor electrode cone is removed and replaced by one designed for use with the Duoplasmatron source. This is necessary because of the differences in source aperture-to-extractor spacing and size. The Duoplasmatron filament arrangement differs from the Danfysik in that it consists of a 1- by 4-in. piece of platinum gauze instead of a coiled tungsten wire between two posts. The edges of the gauze strip are rolled lengthwise toward the center; the strip is then bent into one full loop and each end is attached to an electrode. The gauze filament, before attachment to the electrodes, is dipped in an emission enhancement solution (barium carbonate) and then baked for 3 h at 150°C. The filament assembly is then placed into the magnet and aperture housing.

The completed assembly is then put on the accelerator tube stack. The Duoplasmatron source has only one gas-feed line. The second feed line used with the Danfysik source is plugged when the Duoplasmatron is in use. The electrical connections are similar except for the following: (1) the anode is connected to either of the filament electrodes, (2) the anode power supply polarity must be reversed to negative, (3) the filament voltmeter must be disconnected, and (4) the anode volt and ammeter leads must be reversed. The Duoplasmatron source assembly requires two (upper and lower) coolant flow paths; therefore, an additional inlet and outlet from the coolant lines must be attached.

APPENDIX C

HIGH-FREQUENCY CHOPPED ION BEAMS

Because of the high inertia of heavy ions in the million-electron-volt energy region, we have chosen to carry out high-frequency ion-beam chopping before acceleration by the 5-MV accelerator tube. This was accomplished by chopping the extracted ion beam, whose energy is only about 20 keV. Under direct (unchopped) ion-current conditions, the extracted beam is focused by the einzel lens electrode (see Fig. 4) until it passes through the ExH mass analyzer. The mass analyzer is a Wien velocity filter consisting of a set of parallel plates made of nonmagnetic steel surrounded by a magnetic field. The magnetic- and electric-field lines are adjusted so that only ions of a selected mass can pass without deflection. Undesired ions are deflected so that they miss the entrance aperture to the gap lens preceding the accelerator tube.

Ion-beam chopping in this arrangement was carried out by superimposing (Fig. C.1) a modulating electric field on the otherwise steady-state dc electric field in the Wien filter. The steady field is generated by a dc power supply (A). The magnitude is controlled remotely from the control console and ranges from 0 to 1.5 keV. The ac field is generated by the push-pull chopper (B). The magnitude of the potential is fixed at 225 V peak to peak and is a square wave. The frequency of the chopper is generated by an oscillator (C) with a frequency range of <1 kHz to >50 kHz. AC power to the power supplies (D) for the oscillator and chopper is "floated" by an isolation transformer (E) so that the output produced by the circuitry is added on top of the potential of the dc supply.

The oscillator circuit consists of a CD4047AE CMOS multivibrator IC and associated components. This IC was chosen because it operates in the required range with only a simple RC network to set the frequency; it has good noise immunity and provides two square-wave outputs of 0 and 180° from an internal divide-by-2 flip-flop. The chopper circuit is built around a pair of VN6000KNT VMOS power transistors arranged in series across the 225-V power supply, with the output taken from the midpoint between the two transistors. The 180° difference in the drive to the gates of the VMOS transistors is obtained from the symmetrical divider

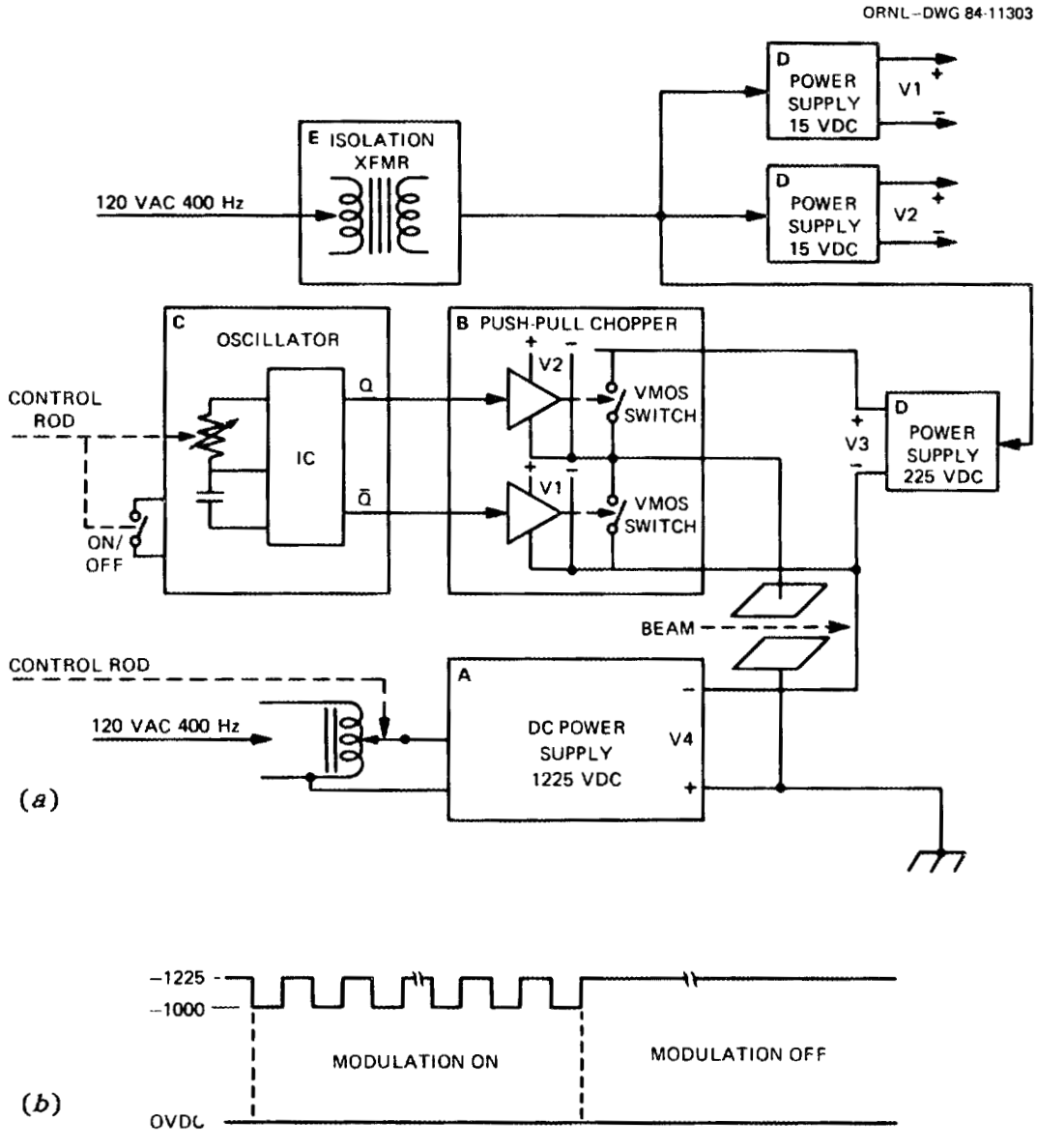

Fig. C.1. (*a*) Schematic drawing of the basic elements in the chopper, (*b*) typical electric field modulation pattern.

outputs of the oscillator IC. Each of the drive signals goes through an optical isolator IC and complementary emitter-follower driver for two reasons: (1) since the path delays are equal, the current that flows through the series transistors at commutation is minimized; (2) the drivers increase the gating signal voltage and current to minimize the switching times and to decrease the on-resistance of the VMOS transistors to optimize performance. The performance of the chopper can be monitored by examining the fine structure of the ion-beam profilometer or a backscattering event.

APPENDIX D

TRANSMISSION ELECTRON MICROSCOPY SPECIMEN LOADING PROCEDURE

1. Clean face plates and thermalizer blocks with alcohol.
2. Place face plate [item (*a*) in Fig. D.1] beam-side down into the loading jig (Fig. D.1), locating the plate's outer notch in a consistent direction (e.g., to the lower right).
3. (Optional) If individual 0.025-mm-thick (0.001-in.) bar masks are to be used to permit postbombardment step-height measurements, load them first in each recess with the bar oriented vertically on the side opposite the outer notch.
4. Load the crushable platinum wire rings (normally 0.125 mm thick), gently pushing them flat, if necessary, with the end of a rod of like diameter.
5. (Optional) To reduce adherence of the platinum wires to soft specimen materials or at high temperatures, insert 0.050-mm-thick stainless steel washers that have been given an oxidized surface finish [item (*d*) in Fig. D.1].
6. Load the specimens face down.
7. Load the specimen that has a thermocouple welded to its face. In lieu of the bar mask and washer of steps 3 and 5, a 0.20-mm-thick platinum gasket wire can be used.
8. Carefully place the thermalizer block, smooth-side down, over the specimens without dislodging them (this is invariably difficult with the thermocouple specimen). The thermocouple holes in the thermalizer block must be oriented properly with respect to the face plate; that is, for the face plate inverted with its outer notch at a 4-o'clock position, as in step 2, the thermalizer block edge holes must be at the 7- and 1-o'clock positions.
9. Apply the hold-down clamp, which locks into position.
10. Removing the knurled index pin, invert the pivoting table. Two of the 2-56- by 1/8-in. socket head screws can be inserted through the face plate and lightly tightened.
11. Invert the pivoting table again, release the hold-down clamp, remove the specimen holder, and install the other two screws.

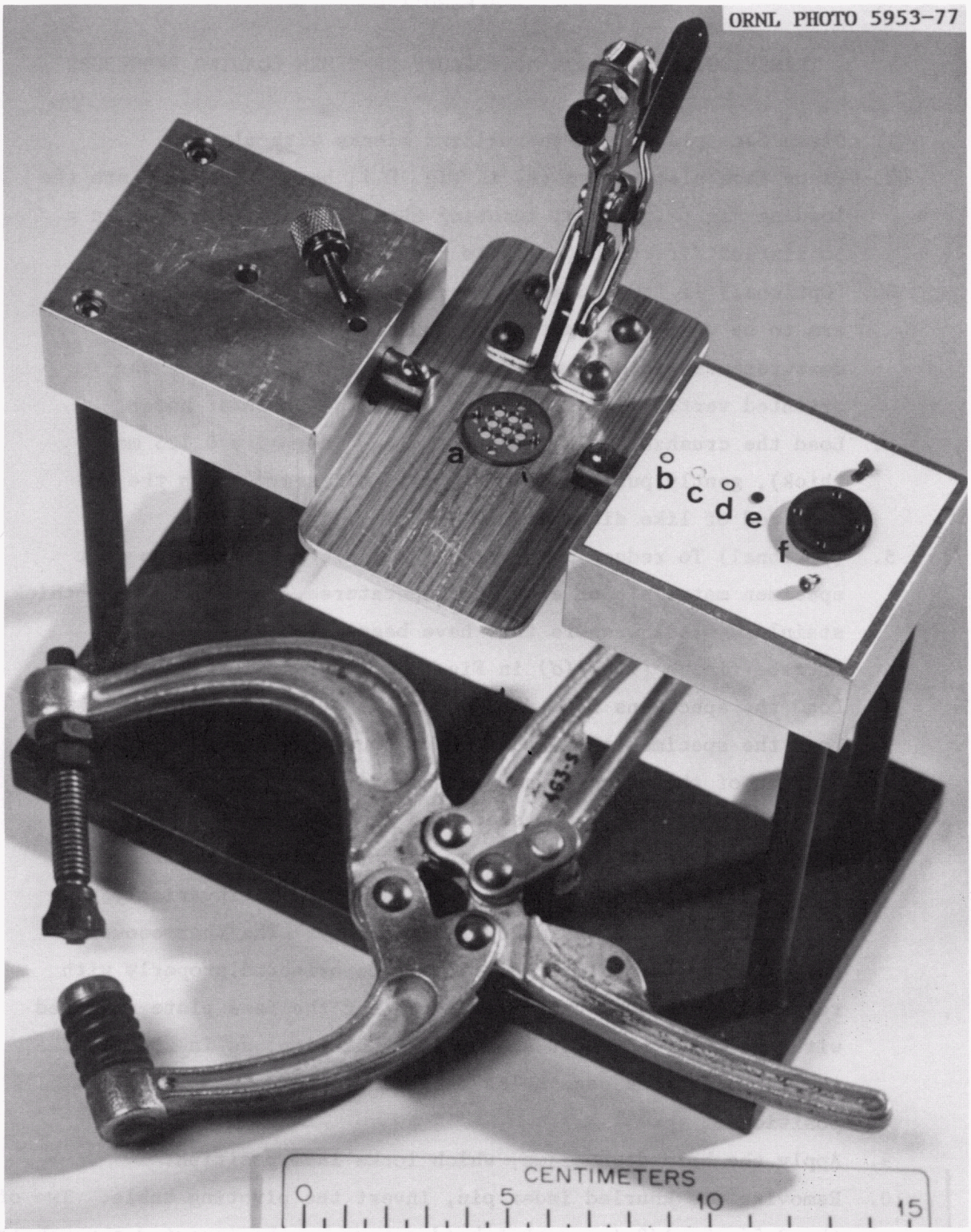

Fig. D.1. Disassembled specimen holder in the loading jig. Components are (*a*) face plane, (*b*) miniature bar mask, (*c*) platinum wire gasket, (*d*) optional 0.05-mm-thick oxidized stainless steel space, (*e*) specimen, and (*f*) thermalizer block.

12. Place the specimen holder between the jaws of the Destaco 463-S clamping plier such that the thermocouple lead and the four socket screw heads align with the cutouts in one anvil. Clamp until the plier locks to apply a preset pressure to the holder for the purpose of deforming the platinum wire gaskets enough to retain all the specimens, even if they differ slightly in thickness. The plier develops more than 400 N (90 lb) of force per 3 mm (1/8 in.) of spring compression.
13. While the holder is so clamped, tighten the four screws to retain this compression. The specimen holder can then be released.
14. Thread the specimen thermocouple wires through a segment about 20 mm (3/4 in.) of the double-hole ceramic insulator. The specimen holder is now ready to load into the target chamber.

APPENDIX E

PROCEDURES FOR ION BEAM ANALYSIS

E.1. ION-SCATTERING ANALYSIS

Pulses originating from ions detected by surface-barrier detectors in the scattering chamber must be converted to digital signals and stored in a histogram in order to produce an energy-dispersive spectrum.

An analog voltage pulse output from the surface-barrier detector is shaped and amplified by an ORTEC Model 142 preamplifier and an ORTEC Model 572 amplifier. The bipolar amplifier output is split for input to a multichannel analyzer (MCA) and a Tektronix Model 465 scope. The voltage of each pulse is related to the kinetic energy of a detected particle in proportion to the number of electron-hole pairs created along its track in the surface-barrier detector. Individual voltage pulses are digitized by a analog-to-digital converter (ADC) and sorted according to signal magnitude into bins (channels) in MCA memory addresses of a fixed voltage width. The amplifier gain determines the energy width per channel. A calibration of pulse height to detected particle energy is made in one of two ways. An ORTEC Model 438 research pulser, previously calibrated with a californium alpha source or the backscattering kinematic surface edges of backscattered million-electron-volt alphas from very thin film layers of gold, silver, and copper on a thick silicon substrate, can be used to establish an energy calibration. Energy spectra can be manipulated by the MCA and stored on floppy diskettes. The unipolar output from the amplifier is routed to an ORTEC Model 550 single channel analyzer (SCA). This path is used to set energy windows in the detected particle energy spectrum. For channeling applications, a specific region of interest in the backscattered energy is chosen for sampling during crystal alignment procedures. The energy-discriminated output of the SCA is sent to an ORTEC Model 771 timer/ counter and ORTEC Model 449 log/lin ratemeter. A log book is used to record spectrum designation, storage diskette volume number, sample examined, ion energy and species, scattering angle, sample orientation, and ion fluence.

E.2. ION CHANNELING ANALYSIS

Ion channeling permits the study of crystalline order and the characterization of crystal structure disordering processes. The crystal to be examined is placed on a precision goniometer at the common center of rotation for the two mutually orthogonal axes of motion. To utilize ion channeling, the target crystal is rocked, or positioned, such that the ion beam direction vector coincides with, or passes through, a low Miller index crystal axis, or plane, of symmetry. Motion through a symmetry direction is referred to as an angular scan. Alignment is accomplished with the assistance of a stereographic map. A stereogram shows the planes that intersect at a major axis and the location of adjacent planes and axes. Often, the Miller indices of the crystalline direction near the surface normal are known. Typically, a major axis lies $<2^{\circ}$ from the crystal surface normal, and 6 to 12 associated major planes intersect at the axis. Alignment relies on the identification of low Miller index planes near the axis. Individual planes are distinguished by a reduction in the backscattered yield (30 to 70% of the random equivalent yield) as the crystal is moved. The reduction in yield for a specific plane is related to the strength of the interplanar atomic potential between adjacent pairs of atomic planes. The interplanar atomic potential is proportional to the areal density of constituent atoms. Thus, the magnitude of the yield reduction for a plane varies with the Miller indices. A similar argument follows for symmetry axes. After a complete scan encompassing a supposed axial direction, a comparative measure of strength and Miller indices can be assigned to individual planes according to the relative yield reduction. As an example, two (011) and two (001) planes, ordered by decreasing relative yield reduction, intersect at the <001> axis for a diamond structured crystal. Once the converging planes are specified, the predicted axis location can be clarified by a succession of angular scans. In the event of an unspecified axis, the assignment of Miller indices to atomic planes can aid in identifying the axis indices. Alignment can be complicated by a significant increase in the crystalline disorder. For example, a single crystal damaged by low-energy heavy-ion irradiation is more complex to align than when in its pristine state.

Figure E.1 displays the alignment diagram for single-crystal <001> silicon. The goniometer used here has orthogonal single-tilt and rotation axes. The axes of rotation and the surface normal lie at the origin of the polar coordinate system of Fig. E.1. To initiate the alignment process, the target surface normal is tilted 6° from the ion-beam direction vector. A brief backscattering spectrum is taken, and an energy window is set with a single-channel analyzer and a pulse generator. The width of the energy window provides a sampled depth within the crystal for alignment purposes. During alignment, the number of backscattered events per unit integrated dose is monitored. For a crystal with regions of disorder, properly setting the upper and lower limits of the energy window can prove critical. The crystal is rotated through 2π, and angles that result in yield reductions are noted. These points are plotted (solid dots in Fig. E.1), and corresponding opposite pairs are joined by lines. (The curvature of the polar coordinate is negligible for locations near the origin.) A first-order estimate of the physical coordinates of the axial direction is assigned to the intersection position of the planes ($\sim 0.7°$ in Fig. E.1). This location is tuned by a series of angular scans.

ORNL-DWG 88-8526

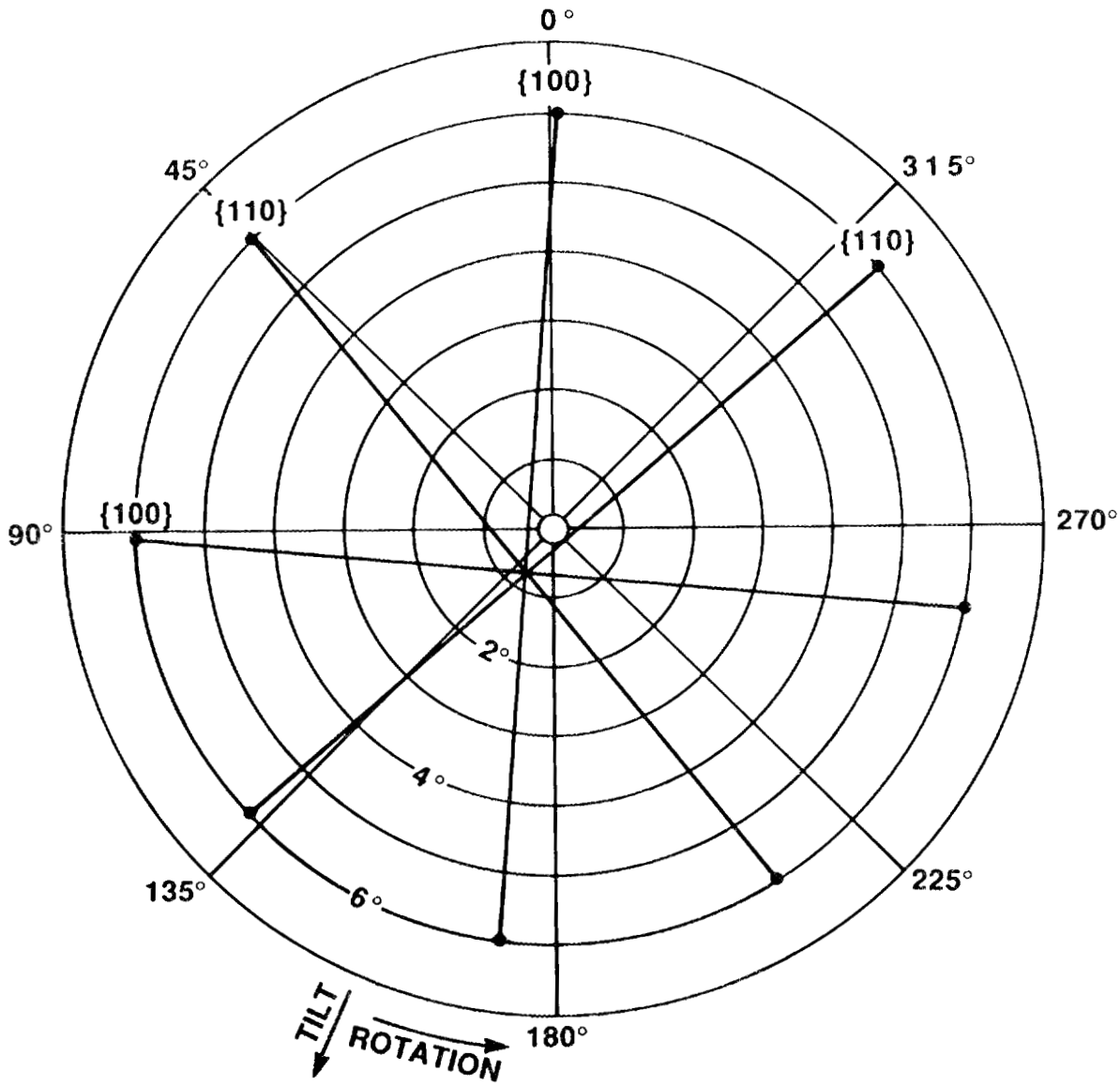

Fig. E.1. Alignment diagram for single-crystal <001> silicon.

APPENDIX F

PROCEDURES FOR AUGER ELECTRON ANALYSIS

When the surface of a target is excited by electron or ion bombardment, part of the emitted radiation is the result of low-energy electrons from the shells of atoms in the first few atomic layers. The energy and intensity analysis of these Auger electrons give clues to the chemical identity of the specimen's surface.

This document is intended as a summary of operating instructions for the Triple Ion Irradiation Laboratory Auger electron spectroscopy (AES) system.

F.1. PRELIMINARY

Power the AES module units and allow a 1-min warm-up period.

F.2. ENERGY CALIBRATION

F.2.1. Auger System Control (Perkin-Elmer Model 11-500A) Settings

Modulation amplitude = 3 eV peak-to-peak
Scale = 20 eV per division
Lower limit = 1950 eV, read on digital meter
Upper limit = 2050 eV
Zero suppress = on and adjusted properly to place energy region of interest (ROI) on TEK screen
Mode = repetitive
Sweep rate = 8 eV/s*10^2

Meter switch allows primary electron beam current to be monitored on the digital meter. Start button begins energy sweep. Hold button pauses energy sweep. Reset button returns scan to lower limit and restarts energy sweep.

F.2.2. Electron Gun Control (Perkin-Elmer Model 11-010) Settings

Power on and allow to warm-up for 5 min

Beam voltage = 2 keV

Raise filament to <1 mA (about five full turns)

Check primary electron current and adjust the filament and emission to optimize at ~25 μA. Observe emission to detect drift of the electron beam current during the progression of time.

Beam voltage may be turned on and off without caution.

F.2.3. Lock-in Amplifier (ORTEC Model 9501) Settings

Time constant - 10 ms

Start Auger control system

Null noise level by putting lock-in signal 90° out of phase

F.2.4. Monitor (Tektronix Model 604)

Adjust intensity and focus to taste

F.2.5. X-Y Recorder (Hewlett Packard Model 7015B)

Remove protective cap from pen

Activate servo mechanism

Zero x and y

Check the pen movement by locating the lower and upper limit positions on the plotting tablet. Be careful not to damage the servo by "pegging" the pen. Lower pen when ready to begin analyses.

F.2.6. Electron Multiplier Supply (Perkin Elmer Model 20-075)

Turn high voltage on

Pressure >7 x 10^{-5} torr for operation

Come up slowly on the voltage (keep below 500 V for electron elastic scattering)

dN/dE signal should appear on the Tektronix monitor as voltage is raised.

Calibrate the target-to-CMA distance to optimize the number of detected Auger electrons with 2-keV elastic recoils.

Maximize the dN(E)/dE signal by adjusting the Vernier calipers that position the sample relative to the CMA source point. The sample surface should be placed at or near the source point of the CMA. The optimum dN(E)/dE signal should be observed for the trace crossover to occur at 2000 eV on the electron kinetic energy axis. Reducing the time constant on the lock-in amplifier decreases the background noise, but with a concomitant reduction in the sensitivity (signal-to-noise ratio).

F.3 SUGGESTIONS FOR ACTUAL SAMPLE ANALYSES

Primary electron energy (E_p) should be three times the Auger peak energy.

E_p = 3 or 5 keV in the PHI Handbook of Standard Auger Spectra,[1] if comparing to those reference tracings.

High-voltage OFF on the electron multiplier supply

Auger system control settings:

Zero suppress = off

Lower limit = 25 eV (do not set to a value <25 eV)

Upper limit = 1000 eV

Sweep rate = 3 eV/s

Scale = 200 eV per division (scaling is in error by a factor of 2)

Mode = single

By adjusting the zero suppress, scale, and upper/lower limits appropriately, other electron kinetic energy regions of interest and sweep intervals can be selected.

Electron gun control settings:

Beam voltage to 3 or 5 keV

High voltage to about 500 V for dN(E)/dE signal to become apparent (~600 V at operation)

High voltage can be turned on and off as needed.

Lock-in amplifier settings: time constant = 0.3 s.

F.4 DEPTH PROFILING

F.4.1. Auger System Control Settings

Mode = multiplex to activate the multiplexing mode of operation

F.4.2. Sputter Gun Control (Varian 981-2046)

Power on. Set the emission to 20 mA for 10 min to outgas the gun filament. Isolate the high vacuum pumping from the chamber and backfill with the sputter ion gas (usually argon) to a pressure of roughly 5×10^{-5} torr. The static pressure has a negligible effect on the operation of the CMA. The focus and x-y deflection should have been previously calibrated to place the CMA electron gun spot at the center of the sputtered crater. The beam energy should be set to between 1 and 3 keV. Normal settings for beam rastering are a scan voltage of 300 V on area 1. The erosion rate is judged as a function of time or integrated current on target, or may be measured postmortem by a diamond stylus profilometer.

F.4.3. Multiplex Control (Perkin-Elmer Model 20-055) Settings

Set set/run switch to any one of the six channels (energy windows), set the lower limit, sensitivity multiplier, and the sweep width. This is done by recording the structure of an Auger spectrum and noting the electron kinetic energy window into which each peak of interest falls. Within each energy window, the multiplex unit records the difference between the maximum and minimum in the dN(E)/dE signal height. The sensitivity multiplier has an order of magnitude of adjustment. Set the time base to the desired number of divisions Per minute for the time axis of the output to the X-Y recorder. To begin, turn the Auger system control on, set the set/run switch to run, activate the sputter gun, and depress the peak-to-peak detection button. The output to the X-Y recorder will be the Auger dN(E)/dE signal as sequentially sampled and plotted as a function of measurement time. As material is removed, the composition of the target will change, for example, during the approach to a heterogenous

layer interface or during preferential sputtering, and new features may appear in the Auger spectrum. If so, the depth profile may be paused and a full Auger spectrum taken to identify the electron kinetic energies of any peaks. Multiplexed energy channels may then be reset to monitor the components associated with the altered concentration.

F.5 POWER DOWN PROCEDURE

Turn high voltage off on electron multiplexer supply first. Leave emission on electron gun control fully clockwise. Leave filament on electron gun control fully counterclockwise. Let cool for 1 h after use prior to venting to dry N_2.

F.6 REFERENCE FOR APPENDIX F

1. L. E. Davis, N. C. MacDonald, P. W. Palmberg, G. E. Raich, and R. E. Weber, *Handbook of Auger Electron Spectroscopy* Physical Electronics Industries, Inc., Eden Prairie, MN, 1978.

ORNL/TM-10867

INTERNAL DISTRIBUTION

1–2. Central Research Library
3. Document Reference Section
4–5. Laboratory Records Department
6. Laboratory Records,ORNL RC
7. ORNL Patent Section
8–10. M&C Records Office
11–15. W. R. Allen
16. J. Bentley
17. D. N. Braski
18–22. R. A. Buhl
23. R. L. Beatty
24. G. L. Copeland
25–29. S. W. Cook
30. D. F. Craig
31. C. K. H. DuBose
32. L. K. Mansur
33. R. E. Clausing
34. L. Heatherly, Jr.
35. R. L. Heestand
36. L. L. Horton
37. T. J. Huxford
38. M. J. Kania
40. H. E. Kim
39. E. A. Kenik
41. E. H. Lee
42–46. M. B. Lewis
47. C. J. McHargue
48. M. K. Miller
49. M. E. O'Hern
50. N. H. Packan
51. R. E. Pawel
52. D. F. Pedraza
53. A. C. Schaffhauser
54. P. S. Sklad
55. R. E. Stoller
56. C. W. White
57. F. W. Wiffen
58. D. F. Wilson
59. M. H. Yoo
60. S. J. Zinkle
61. A. D. Brailsford (Consultant
62. H. D. Brody (Consultant)
63. F. F. Lange (Consultant)
64. D. P. Pope (Consultant)
65. E. R. Thompson (Consultant)
66. J. B. Wachtman, Jr. (Consultant)

EXTERNAL DISTRIBUTION

67. DOE, OAK RIDGE OPERATIONS, P.O. Box 2001, Oak Ridge, TN 37831-8600

Assistant Manager for Energy Research and Development

68–77. DOE, OFFICE OF SCIENTIFIC AND TECHNICAL INFORMATON, Office of Information Services, P.O. Box 62, Oak Ridge, TN 37831

For distribution by microfiche as shown in DOE/TIC-4500, Distribution Category UC-25 (Materials)